UCRL-ID-142533

Dislocation Dynamics: Simulation of Plastic Flow of bcc Metals

D. H. Lassila

February 20, 2001

U.S. Department of Energy

Lawrence
Livermore
National
Laboratory

Approved for public release; further dissemination unlimited

DISCLAIMER

This document was prepared as an account of work sponsored by an agency of the United States Government. Neither the United States Government nor the University of California nor any of their employees, makes any warranty, express or implied, or assumes any legal liability or responsibility for the accuracy, completeness, or usefulness of any information, apparatus, product, or process disclosed, or represents that its use would not infringe privately owned rights. Reference herein to any specific commercial product, process, or service by trade name, trademark, manufacturer, or otherwise, does not necessarily constitute or imply its endorsement, recommendation, or favoring by the United States Government or the University of California. The views and opinions of authors expressed herein do not necessarily state or reflect those of the United States Government or the University of California, and shall not be used for advertising or product endorsement purposes.

This work was performed under the auspices of the U. S. Department of Energy by the University of California, Lawrence Livermore National Laboratory under Contract No. W-7405-Eng-48.

This report has been reproduced directly from the best available copy.

Available electronically at http://www.doc.gov/bridge

Available for a processing fee to U.S. Department of Energy
And its contractors in paper from
U.S. Department of Energy
Office of Scientific and Technical Information
P.O. Box 62
Oak Ridge, TN 37831-0062
Telephone: (865) 576-8401
Facsimile: (865) 576-5728
E-mail: reports@adonis.osti.gov

Available for the sale to the public from
U.S. Department of Commerce
National Technical Information Service
5285 Port Royal Road
Springfield, VA 22161
Telephone: (800) 553-6847
Facsimile: (703) 605-6900
E-mail: orders@ntis.fedworld.gov
Online ordering: http://www.ntis.gov/ordering.htm

OR

Lawrence Livermore National Laboratory
Technical Information Department's Digital Library
http://www.llnl.gov/tid/Library.html

This presentation contains no
classified nor SUI
Reviewed By:

Dislocation Dynamics: Simulation of Plastic Flow of bcc Metals

FY-2000 Final report

David H. Lassila
February 20, 2001

Introduction to final report

This is the final report for the LDRD strategic initiative entitled "Dislocation Dynamic: Simulation of Plastic Flow of bcc Metals" (tracking code: 00-SI-011). This report is comprised of 6 individual sections. The first is an executive summary of the project and describes the overall project goal, which is to establish an experimentally validated 3D dislocation dynamics simulation. This first section also gives some information of LLNL's multi-scale modeling efforts associated with the plasticity of bcc metals, and the role of this LDRD project in the multiscale modeling program. The last five sections of this report are journal articles that were produced during the course of the FY-2000 efforts. The titles, authors and references of these sections are as follows:

- **Connecting the Micro to the Mesoscale: Review and Specific Examples,** V.V. Bulatov (UCRL-JC-135534) Multiscale Phenomena in Plasticity, 259 - 269. J. Lepinoux et al (eds.), 2000
- **Dislocation Multiplication in BCC Molybdenum: A Dislocation Dynamics Simulation**, Moono Rhee, David H. Lassila, Vasily V. Bulatov, Luke Hsiung and Tomas Diaz de la Rubia (UCRL-JC-137147), submitted to Phil. Mag. Let. (2000)
- **Initial dislocation Structure and Dynamic dislocation Multiplication in Mo Single Crystals**, L. M. Hsiung and D. H. Lassila (UCRL-JC-138788) Published in Advances in Computational Engineering & Sciences, Edited by S.N. Alturi and F. W. Brust, Tech Science Press (2000), V. 2, P. 1944. It was also submitted to a special issue of the journal: Computer Modeling in Engineering & Sciences for publication.
- **From forest hardening to strain hardening in body centered cubic single crystals at low temperatures: simulation and modeling**, M. Tang, M.Fivel, L. P. Kubin (UCRL-JC-139714), Journal: Materials Science and Engineering A, in press (2000)
- **Observation of Dislocation Dynamics in the Electron Microscope**, B. W. Lagow, I. M. Robertson, M. Jouiad, D. H. Lassila, T. C. Lee and H. K. Birnbaum. Dislocation-2000 Meeting, Materials Science and Engineering A, in press (2000).

In addition to these publications, there have been several other notable achievements and many others who have contributed to the success of this strategic initiative. In particular the experimental work has lead to the development of unique capabilities for the validation of 3D simulations of the deformation of oriented high-purity single crystals. This work is continuing under programmatic funding and is expected to "test" the predictive capabilities of the simulation codes over a wide range of conditions at ambient pressure. The individuals who have made major contributions to the creation of these experiments include, M. M. LeBlanc, M. Wall, B. Olsen. Also the contributions of A. Goldberg for analyses of crystal purification techniques and J. P. Hirth for valuable discussions and suggestions over the course of this work is gratefully acknowledged.

1.0 Executive Summary

1.1 Multiscale Modeling via Information Passing

Since the development of quantum mechanics great strides have been made in understanding materials phenomena based on "first principles" associated with atomic and sub-atomic structure. Perhaps the most notable examples are in the fields of microelectronics and nuclear energy. In other fields the connections between the fundamental nature of atomic structure and important properties are problematic because in addition to atomic structure, other structural aspects of the material at longer length scales are important. This is the case when considering the mechanical behavior of metals. Although general relationships between composition of metals and their mechanical properties have been established, a detailed understanding of the effects of the composition and microstructure based on first principles is lacking. For example, it is well known that a metal's strength (resistance to change shape during non-reversible plastic deformation) increases if the grain size is decreased however there is no fundamental understanding of this phenomenon.

In recent years there has been increasing interest in using what are termed "multiscale modeling" approaches to understand the effects of composition and microstructure on mechanical behavior. Two fundamental approaches have emerged. The first is essentially a nesting of an atomistic simulation in a continuum computer code simulation. This approach has been used to relate the propagation of cracks to the atomic structure at crack tips by essentially embedding an atomistic simulation within a continuum computer code simulation. The second approach to multiscale modeling is based on information passing between different simulations at various length scales that capture the entire relevant material behavior. In this approach there is a decoupling of length and time scale and, in principle, macroscopic behavior such as a metal forming operation can ultimately be modeled with continuum computer codes with little or no decrease in computational efficiency.

The LLNL multiscale modeling work plan is based on information passing and has been established for modeling the strength properties of body-centered-cubic (bcc) metals. The approach employs three key computer simulations: atomistic, microscale (*dislocation dynamics*) and mesoscale/continuum, as shown in Figure 1. The ultimate goal of LLNL's multiscale modeling efforts is to provide critical information on strength properties for use in continuum computer code simulations.

Dislocation dynamics simulations are the critical link between atomistic simulation and continuum computer codes within the "information passing" scheme and the subject of this strategic initiative. The focus of is on the comprehensive development of an experimentally validated 3-D modeling capability for dislocation dynamics.

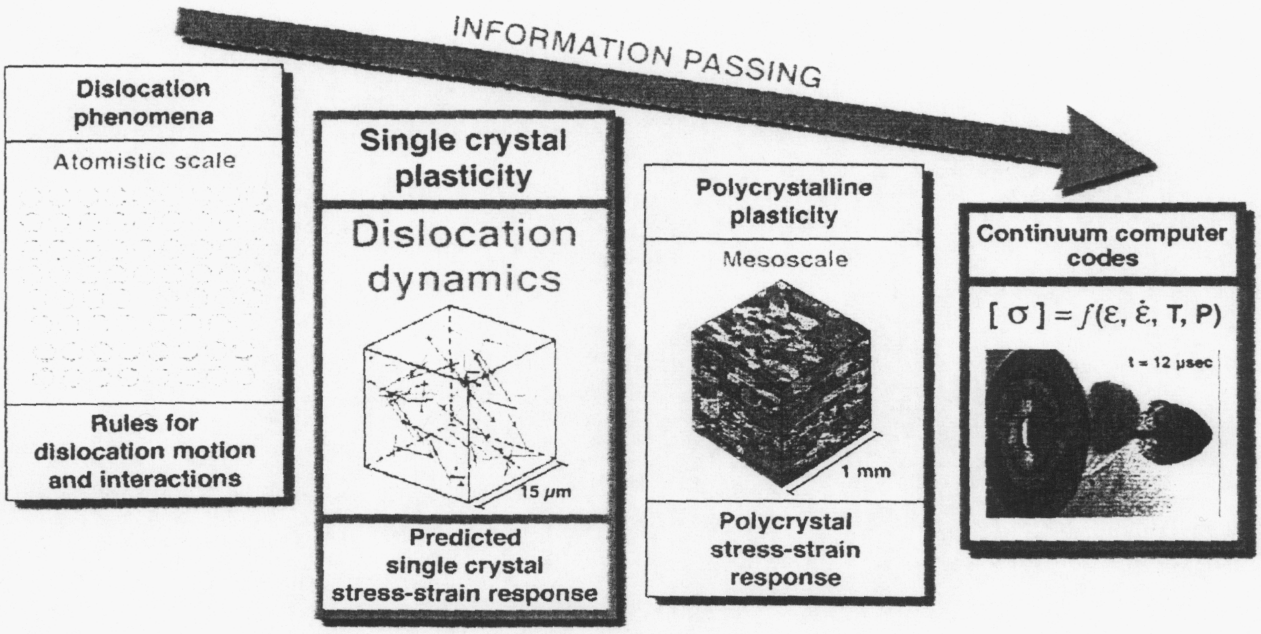
INFORMATION PASSING
Dislocation phenomena
Atomistic scale
Rules for dislocation motion and interactions
Single crystal plasticity
Dislocation dynamics
15 μm
Predicted single crystal stress-strain response
Polycrystalline plasticity
Mesoscale
1 mm
Polycrystal stress-strain response
Continuum computer codes
[σ] = ƒ(ε, ε̇, T, P)
t = 12 μsec

Figure 1. Multiscale modeling of bcc plasticity. The ultimate goal of the modeling program is prediction of the constitutive behavior of bcc metals under extreme conditions of pressure.

1.2 Dislocation Dynamics SI work plan overview

The Dislocation Dynamics SI simulation development and experimental work was focused on the mechanical behavior of molybdenum (Mo), which is a typical bcc metal. The technical work plan involved simulation development and experimental work, and is summarized below.

1.2.1 Simulations

The dislocation dynamics simulations are principally 3-D and are specific to the deformation behavior of bcc metals. The principle objective of the simulation was to produce the plastic deformation, i.e., strength and work-hardening behavior, of single crystal bcc Mo and Ta. This information can be used directly in some strength models currently used in continuum computer code simulations of dynamic deformation. Dislocation dynamic simulations utilize "atomistic" information such as the effects of applied stress on the motion of dislocation cores. By incorporation of all the pertinent "dislocation physics" 3-D dislocation dynamics simulations will account for the aggregate behavior of large numbers of dislocation on the strength and work-hardening behavior of single-crystals. In a sense, dislocation dynamics at the microscale is an analogue of molecular dynamics at the atomic scale, where atoms are replaced by dislocation line segments and force laws and rules for dislocation interactions replace interatomic potentials.

The 3-D dislocation dynamics simulations are computationally intensive and use a wide variety of Laboratory computer hardware. Simulations involving large numbers of dislocation segments (large dislocation density and/or large computational volume) were performed on the most powerful massive parallel processor (MPP) supercomputers. Structuring of the codes for optimal efficiency on MPP machines was pursued in collaboration with individuals at IBM and in the Computation Directorate. Some of the dislocation dynamics simulations were performed on the ASCI Blue computer on as many as 80 processors. It was determined that "scalability" hindered peak performance and that to take full advantage of large scale computing, a new "all-parallel" code must be created.

1.2.2 Experimental

Experimental capabilities in three major areas were developed under this strategic initiative; 1) crystal purification, 2) micro-strain deformation experiments, and 3) in-situ transmission electron microscope (TEM) experiments. Micro-strain deformation experiments and insitu TEM experiments were performed on high-purity Mo. These experiments are central to this work because they provide:

1) initial flow stress response used to probe the physics of dislocation motion,
2) stress-strain response (yield and work-hardening) used to validate simulations, and
3) direct observation of dislocation mobility

Extensive characterizations of the test materials using state-of-the-art microscopy techniques were performed to establish relationships between microstructure-property relationships. Static observations of dislocations and dislocation structures were used to validate structures predicted by dislocation-dynamics simulations. We also performed a number of insitu TEM deformation experiments to observe the motion of dislocations in thin films. In some cases atomic force microscopy (AFM) was used to characterize the surface of deformed materials with 3-D atomic-scale resolution of deformation induced "slip traces" associated with dislocation phenomena. The experimental capabilities developed under the strategic initiative have provided a firm foundation for rigorous validation of the predictive capabilities of 3-D dislocation dynamics simulations.

CONNECTING THE MICRO TO THE MESOSCALE: REVIEW AND SPECIFIC EXAMPLES

V.V. BULATOV
Lawrence Livermore National Laboratory
University of California
Livermore, CA 94550
U.S.A.

1. Introduction

Historically, dislocation are thought of and treated as dual objects. The large lattice distortions inside the core region warrant an atomistic treatment, whereas the slightly distorted crystal outside of the core is well represented within a linear elastic framework. Continuum dislocation theory is powerful and elegant. Yet, it is unable to fully account for the structural differentiation of dislocation behavior, say, within the same crystallography class. The source of these structural variations is mostly in the dislocation core (see [1] for an excellent review).

In the past several years, the gap between the two approaches (atomistic and continuum-mesoscopic) for modeling dislocation behavior has started to close, owing to the overlap of the time and length scales accessible to them [2]. The current trend in dislocation modeling is to try to abstract the local rules of dislocation behavior, including their mobility and interactions, from the atomistic simulations and then incorporate these rules in a properly defined continuum approach, e.g. Dislocation Dynamics. The hope is that, by combining the two descriptions, a truly predictive computational framework can be obtained. For this emerging partnership to develop, some interesting issues need to be resolved concerning both physics and computations. It is from this angle that I will try to discuss several recent developments in atomistic simulations that may have serious implications for connecting atomistic and mesoscopic descriptions of dislocations. These are intended to support my speculations on what can and should be expected from atomistic calculations in the near future, for further development of dislocation theory of crystal plasticity.

2. Single dislocation behavior

Some of the important issues concerning single dislocations are core structure and energetics and the atomic modes of dislocation mobility.

2.1. CORE PROPERITES

Static core properties were analyzed in the past using empirical interatomic potentials [3]. More recently, semi-empirical Tight Binding (TB) and Density Functional Theory (DFT) methods were used to analyze dislocation core in silicon and other semiconductors [4,5]. Silicon, in particular, turned out to be an exceptionally "friendly" material for dislocation modeling. This is mostly due to the relatively low plane-wave cut-off energies (for total energy DFT calculations) that can be used in combination with large (hundreds of atoms) supercells. Because dislocation cores in Si are so extremely narrow, these supercells are sufficient to comfortably accommodate one or two dislocations, without core overlap.

Current capabilities of the DFT methods in combination with the rapidly increasing CPU throughput are becoming sufficient for ever more challenging tasks, such as modeling dislocation cores in BCC transition metals from first principles. The latter is an important target in the context of low temperature/high strain rate yield behavior in these materials determined mostly by the mobility of screw dislocations. The screw mobility, in turn, depends critically on the subtle details of the core structure which is poorly described by the interatomic potentials. In general, core contribution to the line energy (as required for the mesoscopic modeling) can and should be accurately evaluated as a function of dislocation character, using interatomic potentials and TB models and, in a near future, first principles methods. Recent calculations suggest that variations of the line energy with the character angle are non-monotonic [6], showing cusp-like features similar to the dependence of the grain boundary energy on the misorientation angle: the cusps follow the low index line directions (for dislocations), similar to the low sigma mis-orientations (for grain boundaries). For comparison, the elastic part of the line energy depends monotonically on the dislocation character. These angular "core modulations" of the line energy are related to the depth of the Peierls valleys along the low index line directions and should affect the ways in which dislocations move through the lattice.

2.2. DISLOCATION MOBILITY

The major obstacle for realistic modeling of dislocation motion is the gap between the time scales of a typical MD simulation and those of the dislocation motion. Only when dislocation mobility is high, as in FCC metals at high temperatures, and only using computationally inexpensive interatomic potentials, can MD simulations be up to the task. Even in such special cases, in addition to the issue of inaccurate potentials, the electron scattering component of the drag force is missing and should be added separately to the phonon drag as an external parameter. On the other hand, when dislocation mobility is low, as in semiconductors or bcc transition metals (screw dislocations at low temperatures), MD simulations become ineffective – dislocations do not move on the nanosecond time scale of a typical MD simulation run. In such situations, Transition State Theory (TST) is a more appropriate frame for the analysis of infrequent dislocation translations [5].

Activation pathways of the kink mechanisms of dislocation motion in silicon have been studied in considerable detail. One important observation was that kink mechanisms of dislocation motion can be multiple and complex [3,4]. A general methodology for *a priori* analysis of possible kink species in the dislocation core was recently suggested, based on the consideration of broken-symmetries in the dislocation core [7]. Since no three-dimensional kink calculations are required for such an analysis, it can be used to predict geometrical characteristics of the possible kinks using accurate *ab initio* calculations of core structures. For silicon, a complete catalog of kink mechanisms was obtained including kink formation and migration energies. Based on this data, a detailed kinetic Monte Carlo (kMC) model of the dissociated dislocation was developed, combining the atomistic energetics of kink mechanisms in the leading and trailing partials with a full Peach-Koehler treatment of dislocation segment interactions and the stacking fault forces [8]. The results suggest a natural explanation of the low stress anomalies of dislocation mobility in semiconductors, including "the starting stress" and "the weak obstacles" effects. Work is underway to incorporate the atomistic kink mechanisms identified recently for BCC Mo and Ta, in a similar kMC model of screw dislocation motion. This is discussed later in the context of cross-slip.

Motion mechanisms of glissile and sessile jogs are being incorporated in the DD models and deserve to be explored atomistically. Atomistic simulations of the conservative jog motion are straightforward, at approximately the same CPU cost as the 3D simulations of kink mechanisms. On the other hand, simulations of the sessile jogs dragging by screw dislocations will require more effort since vacancy or interstitial production is involved. The barriers for thermal activation of these non-conservative mechanisms are of prime importance and should be obtained by direct atomistic simulations. The results can be used to parameterize jog mobilities in the DD simulations and to replace the approximations currently used for the purpose.

2.3. CROSS-SLIP

In addition to the in-plane mobility just discussed, cross-slip is a mechanism by which dislocation motion becomes three-dimensional. As was recently demonstrated in a DD simulation, collective behavior of large dislocation ensembles is critically dependent on whether or not cross-slip is enabled [9]. For the DD models to become realistic, the cross-slip behavior of screw dislocations should be explored and quantified on an atomistic level. Recently, there has been considerable progress in this area. The most significant advance is due to Rasmussen et al, who explored 3D pathways for dislocation cross-slip in FCC Cu [10]. The results are consistent with the Friedel-Escaig (F-E) cross-slip mechanism in which a dissociated screw dislocation forms a finite length constriction and then re-dissociates into the cross-slip plane. The calculated activation barrier at zero stress is 3.0 eV. Despite the impressive computational machinery engaged in this simulation, the principal issue of the optimal cross-slip path remains unresolved for Cu and other FCC metals. This is because the outcome of the simulation (F-E path) was pre-determined by the symmetry of the initial state and by the choice of optimization method (conjugate gradients). Since it is rather likely that multiple paths for cross-slip exist, e.g. Fleischer mechanism [11] or jog-initiated cross-slip, they all deserve careful examination by direct atomistic simulation.

Cross-slip in BCC metals should be very different because, unlike FCC metals, screw dislocations are not confined to any particular plane by a planar dissociation: atomistic calculations suggest that screw dislocations either have a compact core or show a tendency to a non-planar, three-way extension. Cross-slip in BCC metals is nothing special, since screw dislocations do not have to constrict in the same sense as dislocations in FCC metals and should always have a choice of at least three {110} glide planes. Such behavior, when screw dislocations can translate in several planes, can be responsible for the well-known non-crystallographic "pencil" glide in BCC metals when dislocation motion follows rather accurately the Peach-Koehler force direction. At low to intermediate temperatures, both cross-slip and glide should take place by nucleation and propagation of kink pairs: the only difference between the glide and cross-slip planes is the magnitude of shear stress resolved in each plane along the slip direction, i.e. the Schmid factor. The latter can be exactly the same for two close-packed planes of the <111> zone in which case the dislocation is equally likely to move in either plane. In such cases, kinks and jogs are indistinguishable and can be commonly referred to as "kogs". This situation, when two of the three available glide planes have nearly equal Schmid factors, can have interesting consequences for the motion of screw dislocations. Work is underway to incorporate the energetics of kog mechanisms in a kMC model for screw dislocation motion in BCC metals. Preliminary considerations indicate that dislocations can self-harden by a mechanism in which kogs produced in different planes collide and form pinning points which, in turn, can initiate jog dragging and formation of the debris of point defects and prismatic loops in the wake of dislocation motion.

3. Dislocation interactions

Here several issues of dislocation-dislocation interaction and dislocation-point defect interactions are discussed.

3.1. DISLOCATION COLLISIONS

The now famous cartoon from the Hirth-Lothe book illustrates very well the continuum and atomistic (core) stages in dislocation collisions [12]. The idea of that picture is expressed by a big question mark placed on top of the intersection point, implying that we know very little about the close range collisions when the cores of two intersecting dislocations begin to overlap. Although it remains unclear whether and how much the dislocation core contributes to the behavior of dislocations in collisions, recent atomistic simulations of dislocation reactions provide some interesting insights.

Bulatov et al analyzed results of a large scale MD simulation (by F. Abraham) of FCC solid containing a crack and observed that a Lomer-Cottrell (LC) reaction takes place between the dislocations emitted from the crack tip [13]. Junction formation proceeds by zipping, i.e. motion of the triple node points along the junction line and away from each other. Soon after the junction forms, another very interesting event takes place when a third dislocation approaches the first two, enters in a similar LC reaction with one of them and, subsequently, releases the other one of the two initial partners from the first junction reaction. The end result of such a "three-body" dislocation collision is that one of the two initial partners can continue gliding past the junction. This observation implies that even strong LC junctions are "penetrable" for dislocation glide, through a junction replacement mechanism. In other words, even stable junctions can be destroyed by an incoming flux of primary or secondary dislocations. Subsequently, both elastic and core energy contributions to the energetics of the observed reactions were accurately calculated. When scaled to a typical length of colliding dislocations, say 0.5 microns in a cold-worked Cu, the elastic contribution was found to dominate the reaction energetics, consistent with the basic assumption of the Friedel-Saada line tension model.

Despite an initially repulsive arrangement, the intersection of two dissociated dislocations studied in [14] also produces a LC junction. For this to occur, two leading partial dislocations twist each other very significantly and join in an anti-parallel, locally attractive orientation. Continued forcing of one dislocation through the other results in junction unzipping and, eventually, dislocation cutting and jog formation. That such processes can occur even under constraints of unrealistically high forcing stress (from 400 MPa to 4 GPa) and short lengths of the intersecting lines, is supported by another 3D simulation of repulsive collisions (D. Rodney and R, Phillips, personal communication). It stands to notice that junction formation in both cases is consistent with the simple energy considerations (a modified Saada's rule taking into account the elastic anisotropy and the dislocation characters). The implication is that, when forced in contact, two initially repulsive dislocations can modify their approach trajectories to become locally attractive, which results in an energy reduction. This is achieved by bending either both (Zhou et al) or at least one (Rodney-Phillips) of the interacting partners and re-aligning them along the line of intersection of the two glide planes. It is nearly certain that a sufficiently refined DD simulation, a la Klaus Schwarz [15], would have predicted not only the outcome but also a significant part of the collision trajectory in all three cases of junction formation mentioned above. The only part that such a DD simulation can not handle properly is the specific details of dislocation core transformation during zipping and subsequent cutting. For this atomistic simulations are still required. The question is, should we really mire ourselves in such details? My answer to this is – it depends.

One situation in which core details should be rather unimportant in the dislocation reactions in soft FCC metals. For any given collision, what we must be primarily interested in is its outcome which can be one of the following: dislocations do not get in contact, dislocation approach and stay connected, and dislocation connect and pass through each other[1]. For dislocation lengths of practical interest, the energetics of dislocation collisions is determined nearly entirely by the elastic terms. And this elastic contribution is what matters, for as long as the outcome of a given reaction is governed by its energetics. The latter is likely to be the case in the collisions of the highly mobile glide dislocations in FCC metals. In some other situations, core details may have a significant effect on the junction behavior. As an example, even when the forces on its nodal points dictate junction unzipping, the response to these forces may not be immediate. In Si in particular, there should be a significant lattice resistance to motion of the nodal points along the junction line. At low temperature this resistance can be so high that an unstable junction will remain zipped for a very long time.

---

[1] In cases when dislocation cutting occurs, energy of jog creation comes in the picture. It can be argued however that a fate of a given collision is pre-determined by forces other than cutting and the latter will not change the net outcome [16].

When the junction is stable, the core processes may still influence its behavior. One obvious example is a Lomer-Cottrell junction, which does not move in its {100} glide plane, due to a particular extension of its core into two intersecting {111} planes. It is because of this particular core configuration that the LC junction is expected to lock two parent dislocations, the implication being that the LC lock is absolutely sessile. Or is it? In 2D, motion of an extended LC junction dislocation is indeed nearly impossible. In 3D, however, glide in the {100} plane is possible, owing to the simple fact that all three dislocations involved in the LC reaction are parallel to a single {111} plane. This plane intersects the junction and also happens to be the common cross-slip plane of the parent dislocations. Therefore, if the triple node could move in that common plane, junction could move in its {100} plane, simultaneously pulling two glissile arms into their common cross-slip plane. Such a mechanism is not likely to operate if the node is extended: the energy required to form a constriction is very high in many FCC metals. On the other hand, one of the two triple nodes at the junction ends is often constricted for simple geometrical reasons – such a node is expected to glide relatively easily. Karnthaler [17] reported direct observations of {100} glide and of LC dislocations experiencing sessile-glissile transformations, suggesting that glide of LC locks is indeed possible. Since this behavior can have significant implications for the evolution of dense dislocation tangles in the cell walls, it is important to evaluate the atomistic pathways of nodal glide. So far we have calculated the energy of single kink formation on a LC dislocation in Al, at 0.17 eV, and in Cu, at 1.78 eV. These values indicate that the nodal glide mechanisms can be activated by temperature and stress and that their energetics are strongly dependent on the stacking fault energy.

3.2. DISLOCATION-POINT DEFECTS INTERACTION

Atomistic aspects of dislocation-point defect interactions are even less explored than dislocation-dislocation interactions. Considering the intrinsic defects, vacancies and interstitials, full dynamics simulations are possible in certain situations, especially in view of the current advances in computer hardware and novel algorithms. An interesting example is dislocation motion in irradiated metals, where excess vacancies and interstitials can be present in the form of prismatic loops or stacking-fault tetrahedra. In this case, MD simulations can be effective if mobilities of dislocations and/or prismatic loops are high. In addition to possibly affecting the trajectories of moving dislocations through the elastic dislocation-loop interaction, collisions with prismatic loops can result in various dislocation-loop reactions. Outcomes of such reactions can be very interesting, including formation of super-jogs or enhanced cross-slip. In a way, this is similar to the mentioned above mechanism of debris production by screw dislocations in BCC, but in reverse. Another important target is the rate of dislocation climb, which can be sampled by direct MD simulations in certain cases. However, when climb rates are low, static methods may be more appropriate for obtaining the activation parameters of dislocation climb.

3.3. DISLOCATION-SOLUTE INTERACTIONS

Dislocation interactions with impurities and solute atoms are an area of great importance. In most practical situations, dislocation behavior is considerably different in the realistically "dirty" materials, as opposed to the ideal pure ones. Yield behavior in single crystalline Cu is one well-known example where dislocation mobility can vary by several orders of magnitude, depending on the specimen purity. Although continuum theory has provided considerable insight, our understanding of the physics of dislocation-solute interactions needs improvement and atomistic simulations can play an important role. In particular, non-linear effects of the dislocation core have not been studied in sufficient detail. Also, the core effects can influence dynamics of the Cottrell and Suzuki atmospheres.

The above-mentioned modes of dislocation-defect interactions can be incorporated, at least in principle, in the DD models in the form of re-normalized mobility laws. A more challenging problem is to account for the joint evolution of dislocation and alloy microstructures, especially in multi-component alloys and at large solute concentrations. Very little is known about possible synergistic mechanisms by which dislocations can be sources of partial local ordering or new phase formation and the emerging alloy microstructure can affect dislocation behavior. Methods of cluster-variation and semi-grand-canonical Monte Carlo appear to be good choices for exploring the thermodynamics of these processes. The major difficulty, in addition to the mentioned general problem of length and time scales, is the lack of reliable and computationally efficient models of interactions between the host lattice and the impurity atoms. In the hierarchy of models, from empirical potentials, to semi-empirical TB and *ab initio* methods, one has to choose between reliability and efficiency. At present, the semi-empirical TB approaches often provide a reasonable compromise.

4. Summary

Current attempts to develop physically based descriptions of crystal plasticity raise the issue of linking atomistic and mesoscopic (continuum) descriptions of dislocation behavior. For new combined approaches to be predictive, rules for mesoscale simulations should be accurately matched to the atomistic mechanisms. This matching idea poses several general questions starting with the choice of degrees of freedom (DOFs) for setting up a mesoscale dislocation model. A "common sense" principle for selecting a particular mesoscopic representation is that, whatever DOFs are chosen, they must be identifiable both at the atomistic and the mesoscopic levels. In addition, the representation should retain maximum of the essential features of dislocation configurations at a minimal cost, to cut on the number of DOFs.

At present, several representations of dislocation lines have been advanced, including on- and off-lattice discretizations, linear and curved segments, various nodal representations, etc. Some of these map more naturally on the atomistic models while others offer computational advantages. Whatever scheme is used, matching between atomistic and mesoscopic descriptions involves two major aspects: (1) matching of the energies and forces acting on the chosen DOFs and (2) matching of the response of these DOFs to their conjugate forces. It appears that in most situations of practical interest, the forces on the mesoscopic DOFs (segments or nodes) come almost exclusively from the elastic terms. At the same time, the kinetics of dislocation response to these elastic forces resides with the dislocation core. Consequently, an accurate treatment of elastic interactions, including general anisotropy, is more important for obtaining the forces acting on dislocations. On the other hand, atomistic simulations can and should be used more to provide the rules for dislocation response to the elastic forces.

These and other issues can be addressed more effectively if continuum and atomistic modeling efforts are developed in parallel and the meso- and micro-modelers work alongside and interact continuously. The next 5-15 years are likely to produce new developments along these lines. From my own narrow viewpoint, I would like to see significant activities in the following areas of atomistic modeling:

(1) accurate evaluation of dislocation core structure and core energy, with increasing use of TB and DFT methods (semiconductors, BCC transition metals);

(2) MD simulations of dislocation motion, including kink and conservative jog mechanisms and cross-slip (using empirical interatomic potentials and, possibly, TB potentials);

(3) 3D modeling of dislocation junction behavior (static and dynamic, mostly with empirical potentials);

(4) 3D modeling of dislocation interaction with intrinsic point defects, including jog-dragging and debris loop production (static and dynamic, with empirical potentials and TB);

(5) thermodynamics of dislocation-solute interactions and stress-induced phase transformation in metallic alloys (TB and DFT).

In a longer run, I do not expect that the inevitable growth of CPU power will result in a straightforward increase of the system sizes attempting to simulate more and more complex dislocation arrangements. I think this kind of growth better be relegated to the mesoscale DD approaches. Rather, atomistic modeling should concentrate on the "unit" mechanisms of dislocation behavior but use more and more accurate (and CPU intensive) methods for the purpose. To see what may become possible let's assume that the Moore's law will remain accurate for the next 30 years, i.e. that the CPU speed will continue to increase by an order of magnitude roughly every 5 years. Let's take, as a very crude estimate, that the time step per atom is 1000 times costlier for an O(N) TB calculation than for a typical empirical potential, and that the same ratio will hold in the future between the O(N) DFT calculations and the O(N) TB methods. Then, TB calculations should be able to handle the problems of the same complexity as the present day simulations with empirical potentials, but with a time lag of 15 years, followed by the O(N) DFT methods, another 15 years behind.

5. References

1. Duesbery, M.S. and Richardson, G.Y. (1991) The dislocation core in crystalline materials, *Solid State and Materials Sciences* **17**, 1-46.
2. Bulatov, V.V. and Kubin, L.P. (1999) Dislocation modeling at atomistic and mesoscopic scales, *Current Opinion in Solid State & Materials Science* **3**, 558-561.
3. Bulatov, V.V., Yip, S., and Argon, A.S. (1995) Atomic model of dislocation mobility in silicon, *Philos. Mag.* **A 72**, 453-496.
4. Nunes, R.W., Bennetto, J., and Vanderbilt, D. (1998) Atomic Structure of dislocation kinks in silicon, *Phys. Rev.* **B 57**, 10388-10397.
5. Valladares, A., White, J.A., and Sutton, A.P. (1998) First principles simulations of the structure, formation, and migration energies of kinks on the 90o partial dislocation in silicon, *Phys. Rev. Lett.* **81**, 4903-4906.
6. Bulatov, V.V. (1997) unpublished.
7. Bulatov, V.V., Justo, J.F., Cai, W., and Yip, S. (1997) Kink asymmetry and multiplicity in dislocation cores, *Phys. Rev. Lett.* **79**, 5042-5045.

8. Cai, W., Bulatov, V.V., Justo, J.F., Yip, S., and Argon, A.S. (1999) Dynamics of dissociated dislocations in Si: a micro-meso simulation methodology, in V.V. Bulatov, Diaz de la Rubia, T., Phillips, R., Kaxiras, E., and Ghoniem, N. (eds.), *Multiscale Modeling of Materials*, Materials Research Society, Warrendale, pp. 69-76.
9. Devincre, B, and Kubin, L.P. (1997) Mesoscopic simulations of dislocations and plasticity, *Mater. Sci. Eng.* **A 234-236**, 8-14.
10. Rasmussen, T., Jacobsen, K.W., Leffers, T., and Pedersen, O.B. (1997) Simulations of the atomic structure, energetics and cross-slip of screw dislocations in copper, *Phys. Rev.* **B 56**, 2977-2990.
11. Fleischer, R.L. (1959) Cross slip of extended dislocations, *Acta Metall.* **7**, 134-135.
12. Hirth, J.P. and Lothe, J. (1982) *Theory of Dislocations*, 2nd edition, McGraw Hill, New York, p. 793.
13. Bulatov, V.V., Abraham, F.F., Kubin, L.P., Devincre, B., and Yip, S. (1998) Connecting atomistic and mesoscale simulations of crystal plasticity, *Nature* **391**, 669-672.
14. Zhou, S.J., Preston, D.L., Lomdahl, P.S., and Beazley, D.M. (1998) Large-scale Molecular Dynamics simulations of dislocation intersection in copper, *Science* **279**, 1525-1527.
15. Schwarz, K.W. and LeGoues, F.K. (1997) Dislocation patterns in strained layers from sources in parallel glide planes, *Phys. Rev. Lett.* **79**, 1877-1880.
16. Baird, J.D. and Gale, B. (1965) Attractive dislocation intersections and work hardening in metals, *Proc. Roy. Soc.* **257** **A**, 553-591.
17. Karnthaler, H.P. (1978) The study of glide on {001} planes in f.c.c. metals deformed at room temperature, *Philos. Mag.* **A 38**, 141-156.

Dislocation Multiplication in BCC Molybdenum: A Dislocation Dynamics Simulation

Moono Rhee, David H. Lassila, Vasily V. Bulatov, Luke Hsiung and Tomas Diaz de la Rubia

Lawrence Livermore National Laboratory
Livermore, California 94550, USA

Abstract

Plastic deformation of Mo single crystals is examined by direct simulation of dislocation dynamics under stress. Initial dislocation populations are made to mimic real dislocation microstructures observed in TEM cross-sections of pure annealed Mo single crystals. No a priori sources for dislocation multiplication are introduced, yet multiplication takes place through a sequence involving aggregation of grown-in superjogs, bowing of initially-screw segments, and fast lateral motion of edge segments, producing large number of elongated loops and a characteristic cross-grid pattern of screw dislocations.

Since the initial discovery of dislocations in 1934 (Orowan, Polanyi, Taylor), it has been realized that crystal plasticity properties are derivable, in principle, from the aggregate behavior of large collections of crystal dislocations. However, a quantitative connection between dislocation theory and the phenomenology of crystal plasticity is yet to be established, owing to the immense computational complexity of having to deal with large groups of dislocations and the multitude of their physical behaviors. Starting in the early 90s, the realization that bigger, faster computers may be used for crystal plasticity simulations has led to the development of a powerful computational methodology of Dislocation Dynamics (DD) (Kubin et al. 1992). The predictive power of various DD implementations available today is based on their ability to incorporate, in a computationally tractable manner, multiple and complex mechanisms of dislocation behavior.

On one hand, the current trend in DD simulations is to let dislocations behave most naturally (Schwarz and Tersoff 1996, Rhee et al. 1998). On the other hand, computational limitations often dictate that simplified rules for dislocation unit processes be adopted (Kubin et al. 1992). One of the key uncertainties in the DD simulations is how dislocations multiply. Up to now, several ingenious mechanisms for dislocation multiplication have been suggested and, in some cases, experimentally verified. Typically, multiplication is thought to take place when a dislocation attains a certain special configuration. In particular, the famous Frank--Read (FR) mechanism requires the ends of an otherwise mobile dislocation to be pinned (constrained) to the lattice, leaving the nature of such pinning points unspecified. In view of such uncertainties, dislocation sources are usually introduced in the DD simulations in an ad hoc manner, by creating appropriate constrained dislocation configurations by hand. Such simplifications, while often unavoidable, sweep under the rug yet another important issue, namely how dislocation sources themselves form during deformation. Stated alternatively, one may ask what features in the original (undeformed) dislocation microstructure and which dislocation mechanisms conspire to create the necessary multiplication sources.

In this letter we report the first results of direct DD simulations of crystal plasticity in bcc Mo in which dislocations are initially arranged to mimic salient features of the real grown-in dislocation microstructures as revealed by transmission electron microscopy (TEM) analysis. In our simulations no ad hoc sources are introduced: instead the dislocations are allowed to evolve naturally under uniaxial compressive stress. Progressive straining of the simulated specimen is then observed to produce multiplication sources through a sequence involving the motion, coalescence and mutual pinning of superjogs. Formed as a result of dislocation multiplication and glide, the resulting dense network of dislocations features a 'cross-grid' pattern characteristic of experimental TEM micrographs of the plastically deformed single crystalline Mo. At the same time, the predicted net plasticity rate is similar to that observed experimentally.

The specimens for mechanical testing and TEM analysis were cut from single crystals of Mo grown along the $[011]$ direction using the float zone method. Prior to testing the specimens were annealed in ultra high vacuum for one hour at $1500^{\circ}C$. The total impurity content was determined to be 200 wt. ppm, with approximately 50 wt. ppm in interstitials (O,C,N,H). To test the net plastic response, a compressive load along the $[118]$ axis was applied. The tests were performed at a constant strain rate of $0.001\,s^{-1}$, at room temperature. Thin foils for TEM analysis were cut from the purified and annealed crystals, before and after deformation. A fragment of a typical TEM micrograph obtained for a $[0\bar{1}1]$--sliced foil of an as--annealed specimen is shown in figure 1(a). As is typical for Mo and other refractory metals, the observed microstructure is dominated by long segments of screw character, although dislocation tangles were also observed on occasion. Somewhat less common is that the screw dislocations contain significant number of edge steps, superjogs and superkinks, formed during growth. Based on the TEM observations the total dislocation density was estimated at 10^7 cm^{-2}.

[Insert figure 1 about here]

The ultimate test of the predictive capabilities of the DD methodology is a simulation of the deformation response of real dislocation microstructures under stress. Ideally, one would want to directly compare the evolution of the same microstructure in a DD simulation and under the transmission electron microscope. However, this is not an option as it is nearly impossible to accurately index and position all the dislocations using in situ TEM, even in the relatively small volumes amenable to computational modeling. The next best thing the TEM analysis can do is to provide statistical parameters of dislocation microstructures, which can then be used to set up DD simulations. Based on examination of a large number of TEM micrographs obtained for various cross-sections of the annealed specimens, we accumulated and analyzed several statistical characteristics of the dislocation shapes in the initial dislocation microstructures.

As a first step towards direct simulation of realistic dislocation microstructures in Mo we used these parameters to generate initial dislocation configurations for DD simulations. The initial configurations were produced using a biased random walk procedure made to conform to the TEM analysis data as follows: (a) total dislocation density was set at 10^7 cm^{-2} and was distributed equally over eight groups of dislocations with $1/2\langle 111\rangle$ Burgers vectors; (b) each dislocation was represented by a random walk trajectory consisting of alternating screw steps (along $\langle 111\rangle$ direction) and edge steps (along six $\langle 112\rangle$ directions); (c) the lengths of the steps were assigned randomly from an exponential distribution with the average length of 550 nm for the screw steps, ten times longer than that for the edge steps, at 55 nm; (d) directions of adjacent edge steps were correlated -- the probability of stepping in the same $\langle 112 \rangle$ direction was made 12 times higher than the probability of stepping in a different $\langle 112 \rangle$ direction. This procedure leaves aside the mechanisms by which these features form on the initial grown-in and annealed dislocations. It is only designed to reproduce these features, regardless of their origin.

To ensure computational efficiency of the subsequent DD simulations we truncated both the screw and edge exponential distributions to eliminate all the segments shorter than 100 b, or 27 nm. A thin slice through one of the so-generated dislocation microstructures is shown in figure 1(b) and should be compared to the TEM micrograph, figure 1(a). Prior to straining, the simulated dislocations were allowed to move in response to the interaction forces until these forces were relaxed to an acceptable level, below the lattice friction stress. Such 'pre--annealed' simulated specimens displayed noticeable but minor changes in the statistical parameters. The resulting relaxed configurations were then regarded as statistically equivalent to the annealed TEM microstructures.

To simulate plastic response in the bulk of single crystal Mo we used the micro3D code, an efficient off-lattice implementation of the DD approach (for details, see Zbib, Rhee and Hirth 1994, 1996, 1998). An initial 'pre-annealed' dislocation microstructure was generated in a $10 \leftrightarrow 10 \leftrightarrow 10\ \mu m^3$ box using the two-stage procedure described above. Then, uniaxial compression along the [118] axis was applied at a constant strain rate of 1 s^{-1}, at 300 K. The total Peach--Koehler force acting on a given dislocation segment includes two major contributions: the line tension force which opposes any increase of the dislocation line length, and the force exerted on the segment by the local elastic stress. The latter is a combination of the external (uniform) stress and the internal (non-uniform) stress due to elastic interaction with all the other dislocation segments in the simulation volume. Evaluation of these long-range elastic interaction terms presents the bottleneck of the DD simulations. To accelerate the stress updates we used a fast multipole method (Zbib et al. 1996).

Glide of dislocations is the most common manifestation of plastic deformation, while climb is a thermally activated process requiring transport of mass by diffusion and, therefore, is very limited at low temperatures. There are a number of forms (Johnson and Gilman 1959, Kocks et al. 1975, Hirth and Lothe 1992) for mathematically based constitutive relations for the magnitude of the glide velocity v_g. However, in a number of cases of pure phonon/electron damping control, or of glide over the Peierls barrier, a linear form for glide velocity v_g predicts the results very well. That is,

$$v_g = Mb(\tau - \tau_f)\,, \tag{1}$$

where M is the temperature-dependent dislocation glide mobility and climb mobility respectively, τ is the effective shear stress, τ_f is friction stress, and b is the Burgers vector. We adopt this simple form for initial calculations, although an extension to a power--law form can be readily implemented (Prekel and Conrad 1968, Leiko et al 1974, 1975). To account for the anisotropy of dislocation motion in BCC molybdenum we used two different sets of mobility parameters for screw and non-screw dislocations. Specifically, the friction stress τ_f for screw dislocations was set at 26 MPa, 20 times higher than the friction stress for the non-screw dislocations. Likewise, mobility coefficient M for the screws was set at $1\ (\text{Pa ?sec})^{-1}$, 100 times lower than that for the non--screw dislocations (Urabe and Weertman 1975). To handle the events of dislocation exit from and re--entry to the simulation box, reflection boundary conditions were applied (Zbib et al. 1998). Connection between the stress and the strain comes through the rate of plastic strain increase produced by dislocation unit processes. The observed stress--strain curve is then a result of the dynamic equilibrium between the external straining conditions and the internal rate of dislocation multiplication and motion. In the present simulations we decided against introducing any preexisting sources, hoping to examine what kind of plastic response the initial dislocation microstructure itself can produce.

[Insert figure 2 about here]

The dislocation arrangement attained during the DD simulation is shown in figure 2(a), along with the overall stress-strain response in figure 2(b). The latter shows a well-resolved plastic yield behavior, with the yield stress of 130 MPa, in reasonable agreement with experimental observations (Lassila and others 1999). The characteristic cross-grid pattern is also clearly observed and should be compared with a TEM micrograph of the deformed specimen, figure 2(c). The cross-grid consists of two sets of intersecting screw dislocations with $1/2[111]$ and $1/2[11\bar{1}]$ Burgers vectors, respectively, viewed plane-on along the $[\bar{1}01]$ direction. In the course of the deformation, the net dislocation density increased four--fold. What is remarkable is that no dislocation sources were introduced in the initial microstructure and yet multiplication has clearly taken place.

[Insert Figure 3 about here]

To examine the multiplication mechanisms in more detail, we performed a series of simpler simulations in which all but one dislocation, randomly selected from the same initial microstructure, were removed from the simulation box. The remaining dislocation was then subjected to a constant uniaxial stress applied along the $[001]$ axis. The result shown in figure 3(a)-3(f) suggests that, under stress of 200 MPa, multiplication sources develop even on a single dislocation. The sequence begins with the motion of edge superjogs along the dislocation line. The superjogs moving in the same glide plane and in the same direction merge, occasionally forming larger superjogs. At the same time, superjogs gliding on two different planes can move in opposite directions, collide, and form topologically constrained configurations consisting of two superjogs unable to glide past each other. These pinning points chop dislocations up into smaller segments and facilitate further superjog pile--up, coalescence and extension. The pinning points can move along the line in response to the unbalanced force exerted by the pile--ups pushing against each other. Figures ccc show that these pinning points last during the entire simulation, suggesting that the looping process around the sources are continuous. The superjog clusters formed by collision and coalescence are in a quasi-equilibrium state under constant loading conditions where dislocations lower internal energy by interaction and motion.

[Insert Figure 4 about here]

At a lower stress (50 MPa) superjog motion and pile-up proceed unabated but multiplication does not occur as shown in Figure 4. The reason for this is that, at such a low stress, the force acting on the screw segments is below the threshold of friction stress. On the other hand, superjogs can still move along the direction of screw dislocation. This is due to the low friction stress for dislocations of edge character. These relatively highly mobile superjogs of edge character continue to move until they become intact with other superjogs from the opposite direction. By themselves, accumulation and coalescence of superjogs in the pile-ups appear to be insufficient for reaching the critical conditions for the source initiation.

[Insert Figure 5 about here]

That screw motion is important for dislocation multiplication is confirmed by the results obtained in a high stress simulation as shown in Figures 5(a)-5(d). Here, dislocations begin to bow out almost immediately after the stress is applied, and continue to bow out and wrap around the superjogs. Consequently, a large number of small dislocation loops are produced by several multiplication sources activated almost simultaneously, resulting in a higher rate of multiplication. The rate at which superjogs move and collide at higher stress is much less than the case of lower stress (200MPa). At higher stress, initial superjogs become temporarily stationary due to the net force balance of bowing-out dislocations around them, giving a lower stress state where "some" superjogs can be single sources without collision. In general, multiplication begins if and when superjog pile-up and coalescence and glide of screw dislocations combine to produce superjogs long enough for the applied stress to overcome the friction stress, line tension, and mutual attraction of dislocation segments, as shown schematically in figure 6(a)-6(c).

[Insert figure 6 about here]

Mechanistic understanding of dislocation multiplication involves two distinctly different issues. On one hand, it is necessary to examine critical configurations for dislocation sources to begin producing fresh dislocations. On the other hand, understanding the scenarios in which such critical configurations can form is just as important. Although the multiplication behavior observed here maybe viewed as being similar to the 'wandering' source mechanism considered earlier by Kubin and his co—workers (Louchet and Kubin 1975, Louchet et al. 1975), the pathways leading to source formation are very different. In the 'wandering source' mechanism, the superjog of critical height required for the source to operate was assumed to be formed by cross-slip. However, our simulations suggest a different scenario in which stress-induced migration and coalescence of like-sign superjogs result in gradual build-up of larger superjogs, similar to the mechanism of elementary jog aggregation considered by Louat and Johnson (1962). In both cases, the configuration from which the sources begin to operate consists of two dislocation arms bowing under stress, separated by a superjog whose length exceeds the critical value d_c. The analysis given by Louchet and Kubin (1975) and Lochet et al. (1975) showed that the major source in Mo at low temperatures is due to cross slip at large strains, omitting the detailed information about the initial microstructures. The dynamic source generated by the motion of clusters of superjogs mentioned in this paper is unique because of ability of the superjogs to move along the dislocation line to coalesce, these are distinctly different from the FR or other 'fixed' sources for dislocation multiplication. It is possible that, if the occasional dense tangles of dislocations were accounted for in our simulations, multiplication sources of a different nature would have appeared, including the fixed sources. On the other hand, the features responsible for the occurrence of the wandering sources are realistic for the as-annealed specimens of Mo. This, combined with the fact that the simulated yield stress is close to the experimental value, is significant in indicating that the dynamic multiplication sources formed by the clusters of superjogs alone may be sufficient for dislocation multiplication in deformation conditions explored here.

An important and still unresolved issue in the dislocation theory of crystal plasticity is how much the stress-strain behavior depends on the nature of initial dislocation sources. In a typical DD simulation, sources are introduced in the form of dislocation segments pinned at the ends. The origin of such pinning points is left unspecified, although presumably they can be associated with the nodes of dislocation junctions or impurity precipitates. Sometimes, to avoid the ambiguity associated with unphysical termination of the segments inside the crystal, prismatic loops are introduced (Ghoniem 1998). In both cases, the sources are introduced ad hoc with the purpose of generating large number of dislocations during the early stages of plastic deformation. The argument in support of such an arbitrary construct is that eventually some other natural multiplication mechanisms should take over in the later stages and the simulated system would have no memory of the initial artificial sources. Ironically, the maximum plastic strain a DD simulation can produce has been limited to fractions of one percent where the overall behavior is still sensitive to the nature of the initial dislocation sources. This was exactly why in the present simulations we decided to avoid any ad hoc sources but attempted to faithfully reproduce the initial grown-in dislocation microstructure. Still, the dislocations found a way to multiply producing the overall initial yield behavior similar to the experiment. This observation does not preclude that other types of dislocation sources may become active in appropriate conditions, such as FR sources pinned at precipitate particles. What our results do show is that, when properly accounted for, the initial dislocation microstructure contains the features (superjogs) from which dislocation sources can develop.

In summary, we have examined deformation behavior of BCC metals at room temperature by direct Dislocation Dynamics simulations at the ten-micron scale. Initial dislocation arrangements used in our simulations closely match the statistics of grown-in dislocation microstructures in pure annealed Mo single crystals. Contrary to the common practice of DD simulations, we do not introduce any ad hoc multiplication sources, yet dislocation density increases four-fold during straining. Careful analysis reveals that the sources form in the initial stages of deformation from the grown-in superjogs that can move, coalesce and pin each other under stress. Source operation begins once a critical configuration for line extension is reached, depending on the applied stress. Screw dislocations produced by such sources, form a 'cross-grid' microstructure characteristic of BCC transition metals deformed at low temperatures. Likewise, the overall yield behavior agrees closely with experimental data. Dislocation configurations become more isotropic as the temperature increases. The behavior of the dynamic source at high temperature is not studied in this paper and remains to be investigated. However, one must introduce other important ingredients which affect the dislocation motion at high temperatures, i.e. non--conservative motion caused by diffusion process.

Acknowledgements

One of the authors (MR) would like to thank H. M. Zbib and J.P. Hirth for helpful discussions. This work was performed under the auspices of the U.S. Department of Energy by the Lawrence Livermore National Laboratory under contract number W-7405-ENG-48.

References

Ghoniem, N.M, 1998, Proceedings of the 1st Latin American Summer School on Materials Instabilities, Vaparaiso, Chile, Kluwer Pubs.

Kubin, L.P., Canova, G., Condat, M., Devincre, B., Pontikis, V., and Brechet, Y., 1992, Solid State Phenom., **23-24**, 455.

Kocks, U.F., Argon, A.S., and Ashby, M.F., 1975, Progress in Materials Science, **19**, edited by B. Chalmers, J.W. Christian and T.B. Massalski, (Oxford: Pergamon Press), pp.1

Johnson, W.G., and Gilman, J.J., 1959, J. Appl. Phys., **30**, 129.

Lassila, D.H., and others, 1999, LDRD Strategic Initiative: 1999 Progress Report, Lawrence Livermore National Laboratory.

Leiko, E. B., Lotsko, D.V., Nadgornyi, E.M., and Trefilov, V.I., 1975, Sov. Phys. Solid State, **17**, No. 9, 1814.

Louchet, F., and Kubin, L.P., 1979, Phys. Stat. Sol. (a), **56**, 169.

Louchet, F., Kubin, L.P., and Vesely, D., 1979, Phil. Mag. A, **39** , 433.

Louat, N and Johnson, C.A., 1962, Phil. Mag., **7**, 2051.

Orowan,E., 1934, Z. Phys., **89**, 604.

Polanyi, M., 1934, Z. Phys., **89**, 660.

Prekel, H.L., and Conrad, H., 1968, in Dislocation Dynamics, edited by A.R. Rosenfield, G.T. Hahn, A.L. Bement Jr. and R.I, Jaffe (Seattle, Washington Battle Institute Materials Science Colloquia), pp431-451.

Rhee, M., Zbib H.M., Hirth, J.P., Huang, H., and Diaz de la Rubia, T., 1998, Modelling Simul. Mater. Sci. Eng., **6**, 467.

Schwarz, K.W., and Tersoff, T., 1996, Appl. Phys. Lett., **69**, 1220.

Taylor, G.I., 1934, Proc. Roy. Soc. (London) A, **14**, 362.

Urabe, N., and Weertman, J., 1975, Mater. Sci. Engng., **18**, 41.

Zbib, H.M., Rhee, M., and Hirth, J.P., 1998, Int. J. Mech. Sci., **40**, 113.

Figures

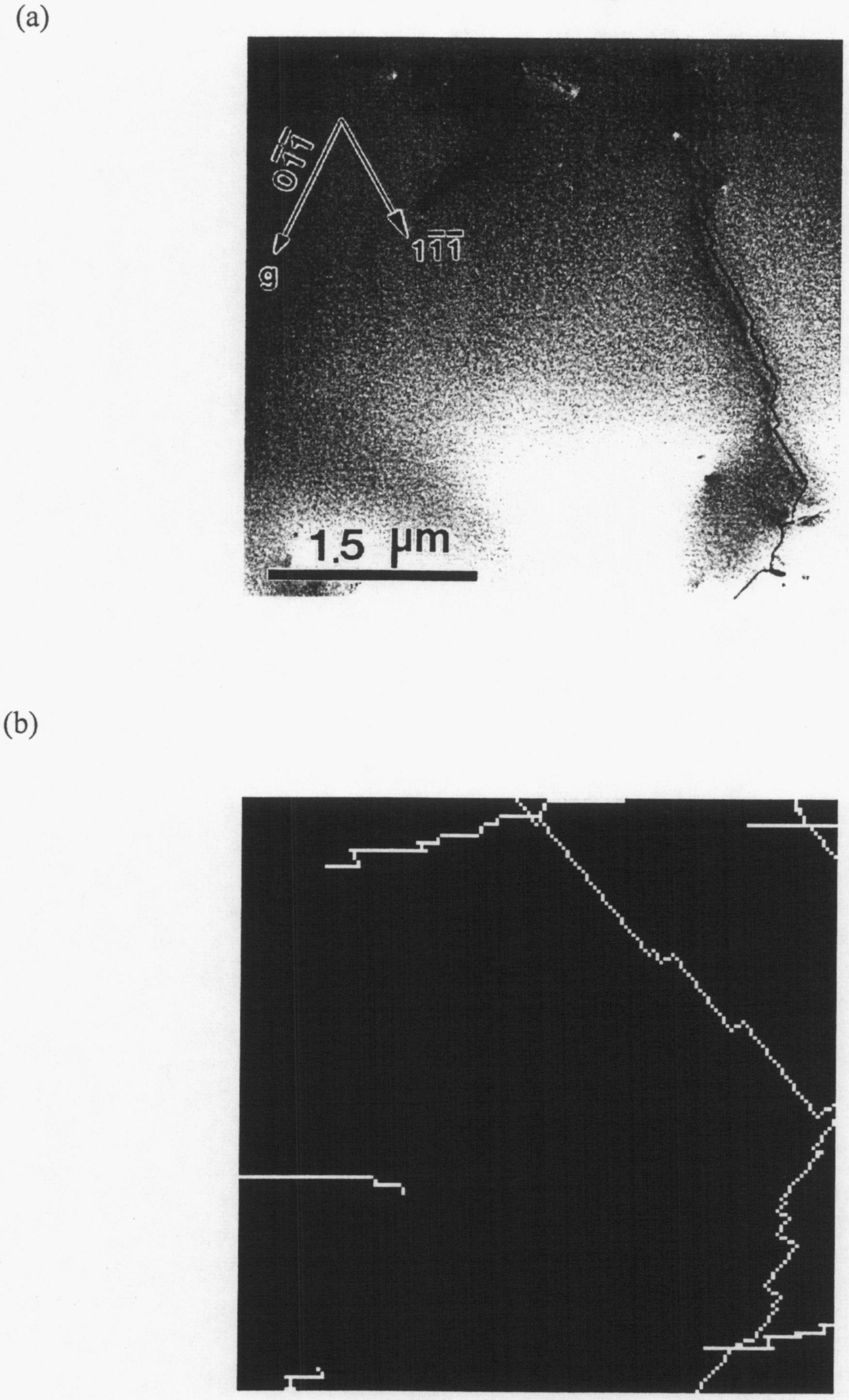
(a)
$0\bar{1}\bar{1}$
g
$1\bar{1}\bar{1}$
1.5 μm
(b)

Figure 1 (a) TEM dislocation microstructure in the annealed Mo, and (b) a sectional view of the simulated microstructure.

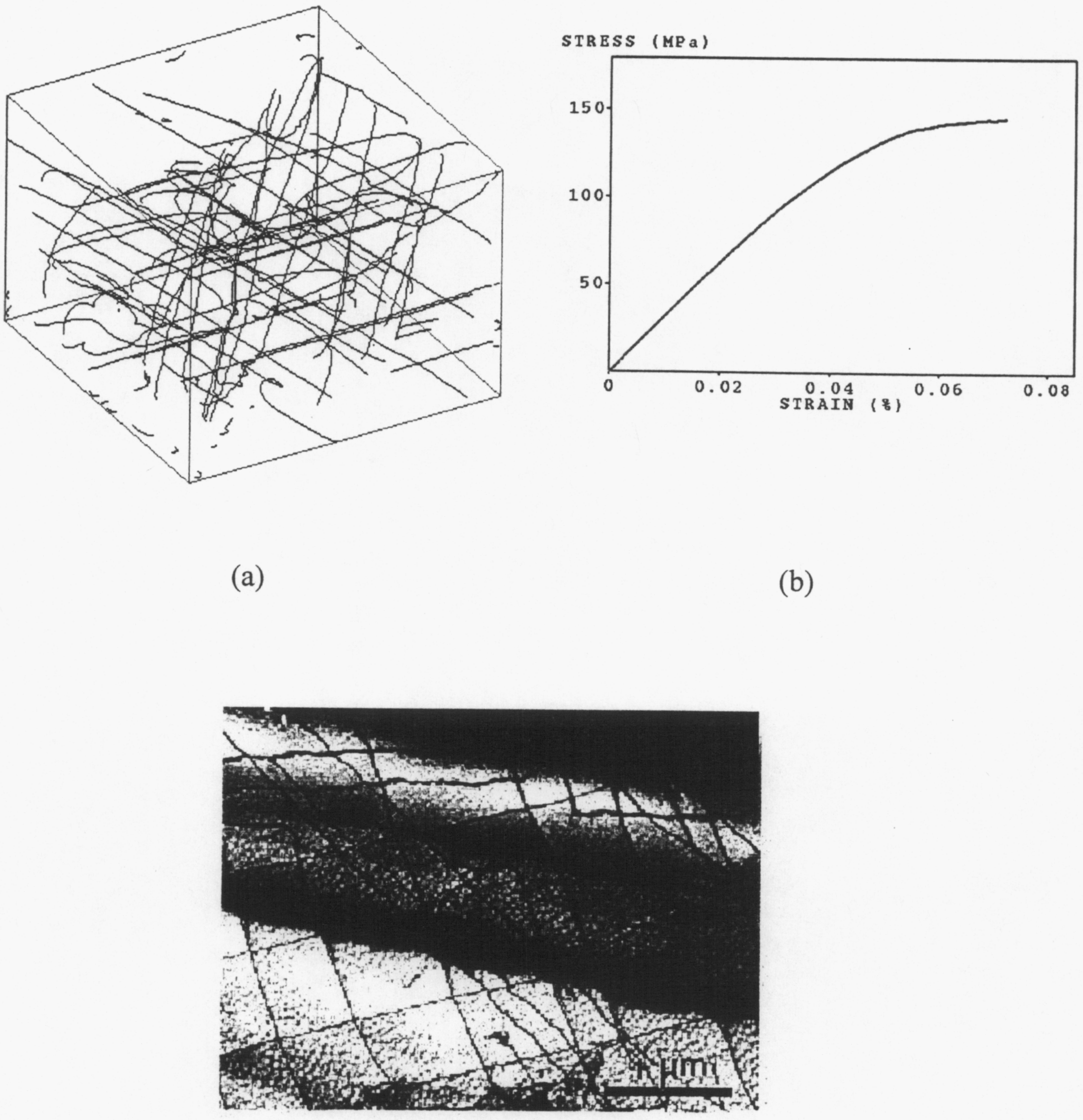

(a)

(b)

(c)

Figure 2

(a) A snapshot of the simulated microstructure, (b) the simulated stress--strain response in the inset, and (c) TEM micrograph showing characteristic cross--grids of screw dislocations.

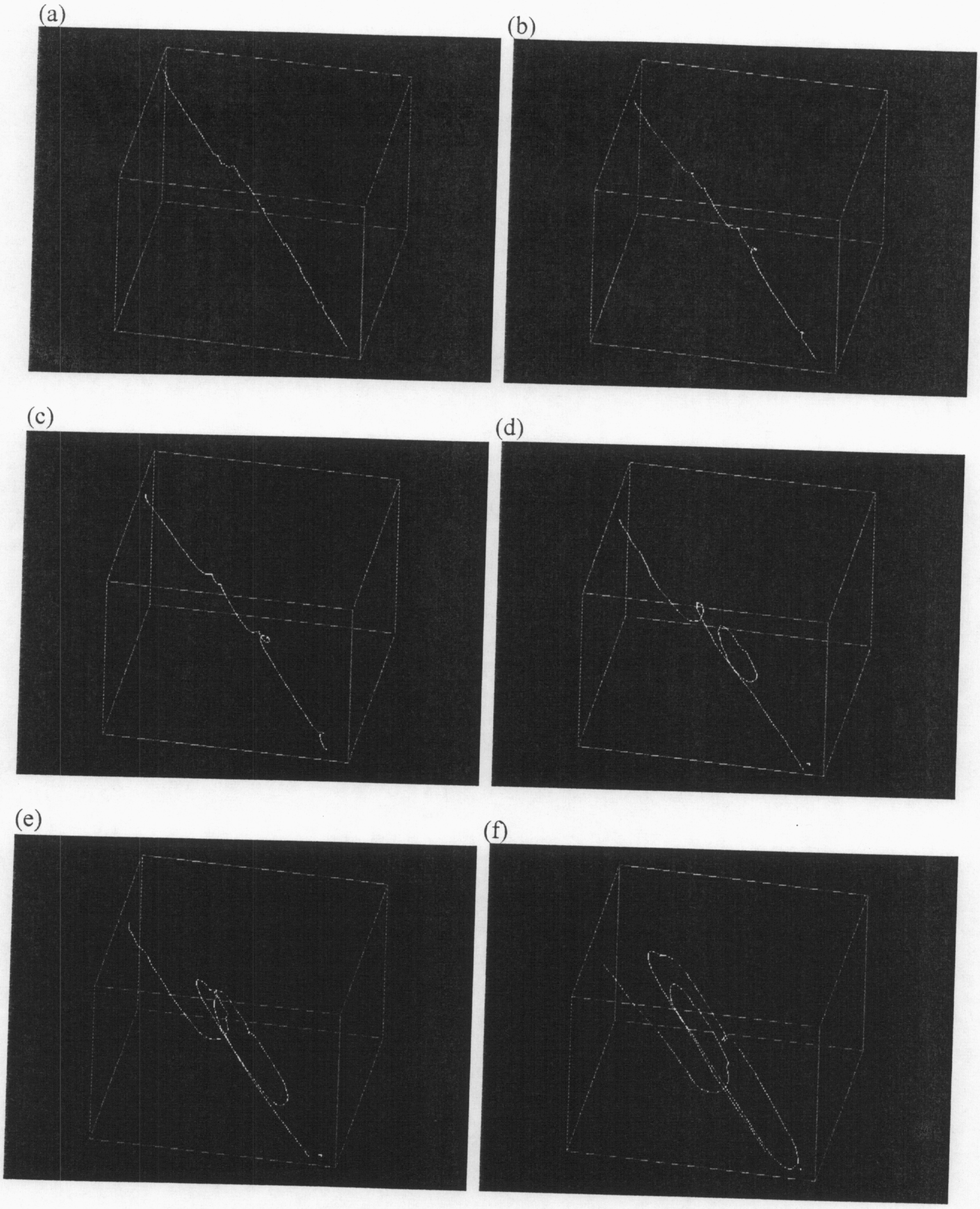

Figure 3 Snapshots of dislocation multiplication sources at 200 MPa along [001].

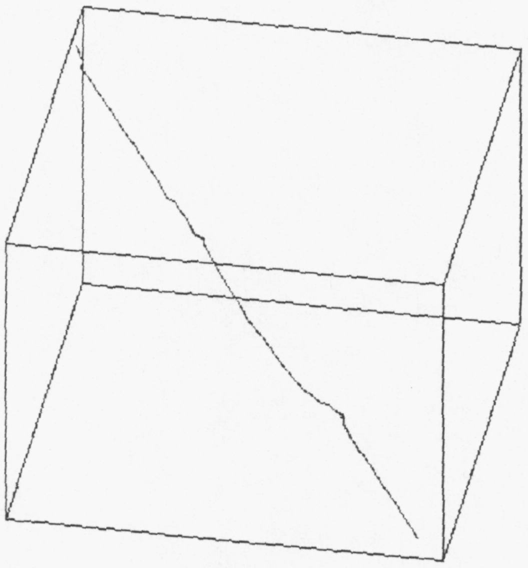

Figure 4 Behavior of a single dislocation at 50 MPa.

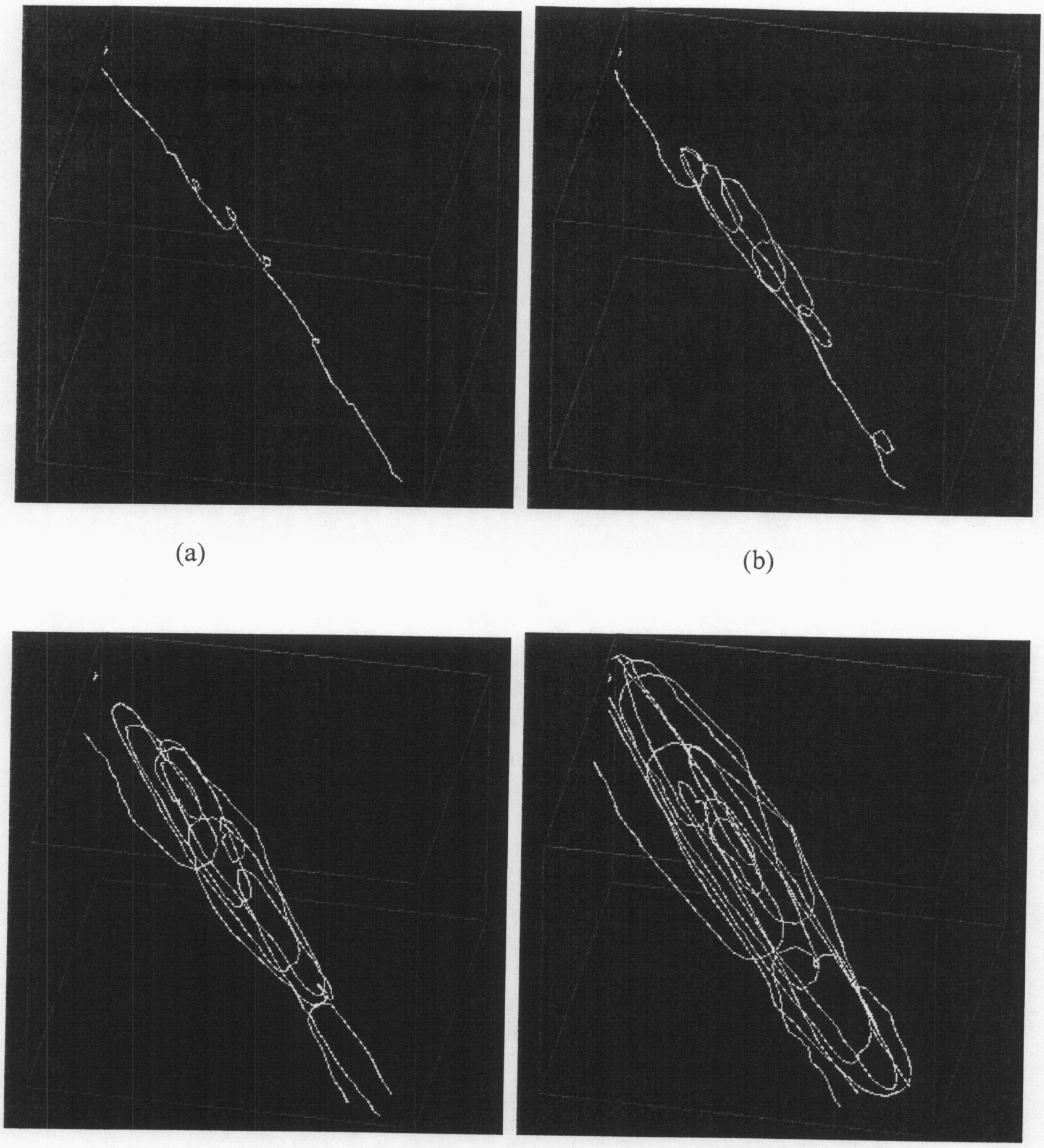

(a) (b)

(c) (d)

Figure 5 Snapshots of behavior of a single dislocation under stress at 1 GPa.

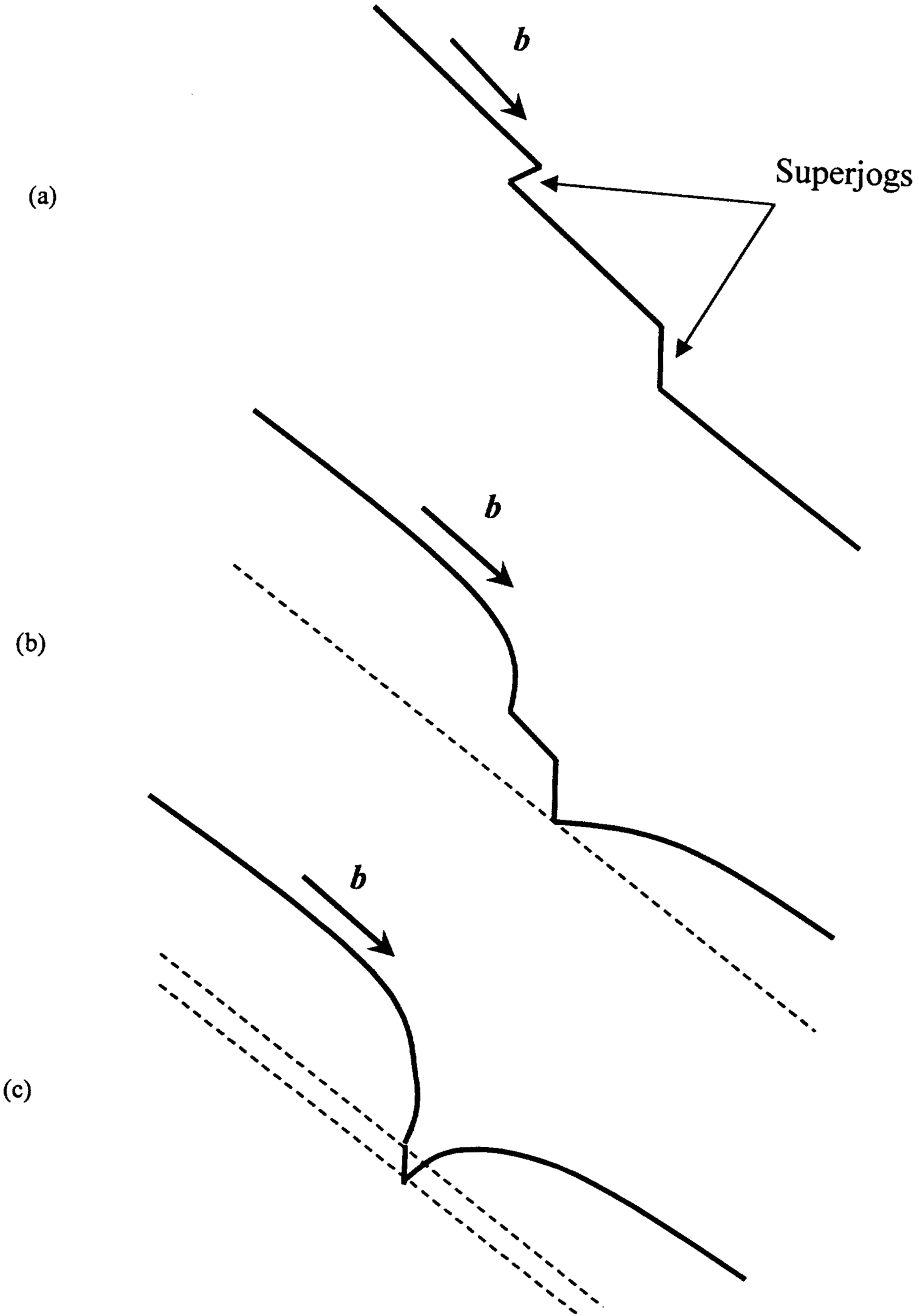
(a)
b
Superjogs
(b)
b
(c)
b

Figure 6 Formation of a pinning point for multiplication source by superjogs under stress.

INITIAL DISLOCATION STRUCTURE AND DYNAMIC DISLOCATION MULTIPLICATION IN Mo SINGLE CRYSTALS

L. M. Hsiung and D. H. Lassila
Lawrence Livermore National Laboratory
Chemistry and Materials Science Directorate
L-352, P.O. Box 808
Livermore, CA 94551-9900

Abstract

Initial dislocation structures in as-annealed high-purity Mo single crystals, and deformation substructures of the crystals compressed at room temperature under different strain rates have been examined and studied in order to elucidate the physical mechanisms of dislocation multiplication and motion in the early stages of plastic deformation. The initial dislocation density was measured to be in a range of $10^6 \sim 10^7$ cm^{-2}. More importantly numerous grown-in superjogs were observed along screw dislocation lines. After testing in compression, dislocation density (mainly screw dislocations) increased to $10^7 \sim 10^8$ cm^{-2}. Besides, the formation of dislocation dipoles (debris) due to the nonconservative motion of jogged screw dislocations was found to be dependent of the strain rates. While little dislocation dipoles (debris) were found in the crystal tested quasi-statically (10^{-3} s^{-1}), more cusps along screw dislocation lines and numerous dislocation dipoles (debris) were observed in the crystal compressed under the strain rate of 1 s^{-1}. Physical mechanisms for dislocation multiplication as well as dipole formation from jogged screw dislocations under different strain rate conditions are accordingly proposed and discussed.

Introduction

Since the initial discovery of dislocations in 1934 [1-3], it has been realized that crystal plasticity properties are derivable, at least in principle, from the aggregate behavior of dislocations. However, a quantitative connection between dislocation theory and the phenomenology of crystal plasticity is yet to be established owing to the immense computational complexity of the task for dealing with a large number of dislocations and the multitude of their physical behaviors. Starting in the early 90's [4], the realization that bigger and faster computers may be used for crystal plasticity simulations has led to the development of a powerful computational methodology for dislocation dynamics (DD). The predictive power of the various DD implementations available today is based on their ability to incorporate, in a computationally tractable manner, multiple and complex mechanisms of dislocation behavior. While the current trend in DD simulations is to let dislocations behave most naturally [5,6], computational limitations often dictate that simplified rules for dislocation unit processes to be adopted [4]. One of the key uncertainties in the DD simulations is how dislocations multiply and move during plastic deformation. To date, several dislocation multiplication mechanisms have been proposed in literature. Typically, dislocation multiplication is considered to take place when a dislocation attains a certain configuration. For example, the well-known Frank-Read (FR) source [7] requires a configuration that both ends of a mobile dislocation segment be pinned (constrained) at two points as a result of either dislocation network or dislocation bend. However, because of an ill-defined nature of pinning points for dislocation multiplication, dislocation sources are usually introduced in the DD simulations in a presumption or an ad hoc manner by setting up a constrained dislocation configuration, which is most often unrealistic. For instance, the initial dislocation configuration for an FR multiplication source may be simply given as a dislocation segment linked between two pinning points with an arbitrarily given length, and dislocation multiplication may thus be mimic or simulated according to the FR multiplication mechanism.

In order to make the DD simulations for dislocation multiplication more realistic, there is a need to understand the correlation between initial dislocation structures (dislocation density, dislocation configuration, free dislocation link length, and grown-in jogs...) and dislocation multiplication during plastic deformation. Accordingly, the main purpose of this investigation is to examine and compare the initial dislocation structures of annealed (high-purity) Mo crystals, and deformation substructures of slightly compressed Mo crystals in order to elucidate the underlying mechanisms of dislocation multiplication and motion during early stages of plastic deformation. Since numerous grown-in superjogs have been observed along dislocation lines within as-annealed Mo crystals, emphasis has been placed upon the strain-rate effect of kink-jog interactions on the dislocation multiplication and motion in the early stages of plastic deformation in Mo single crystals. A preliminary result is reported here.

Experimental

Since the Mo single crystals used for dislocation dynamics experiment must have high purity and low dislocation density in order to establish initial conditions for subsequent dislocation dynamics simulations, the high-purity Mo single crystals were fabricated using a standard electron-beam melting process by Accumet Materials Company, Ossining, NY. The interstitial impurities (ppm in weight) in the as-fabricated crystals are O: 25; N: <10; H: <5; C: <10, respectively. Prior to compression test, the test samples were heat treated at 1500° C for 1 h, 1200° C for 1 h, and 1000° C for 1 h at a vacuum of 8×10^{-11} Torr. Testing of Mo single crystals involves compressing the test samples between two platen surfaces under precise conditions. To measure shear strain during compression, a 3-element rosette gage was bonded in the gage section on each side of the sample. Compression tests were performed on test samples with [118] and $[\bar{2}\ 9\ 20]$ compression axes. These two orientations were originally chosen to investigate deformation behavior associated with the $(\bar{1}\bar{1}2)[111]$ and $(\bar{1}01)[111]$ slip systems, respectively. The samples were compressed at a normal strain rate of 10^{-3} s^{-1} for the [118]-oriented sample, and 1 s^{-1} for the $[\bar{2}\ 9\ 20]$-oriented sample, and both samples were compressed to a value of ~1% axial strain. TEM foils were sliced from the gage section of the tested piece with the foil sliced parallel to the $(\bar{1}\bar{1}2)$ plane from [118]-oriented sample, and the $(\bar{1}01)$ plane for the $[\bar{2}\ 9\ 20]$-oriented sample. TEM specimens were finally prepared by a standard twinjet electropolishing technique in a solution of 75 vol.% ethanol and 25 vol.% sulfuric acid at ~25 V and -10° C.

Results and Discussion

Initial dislocation structures

Figure 1 shows the initial dislocation structures observed from the [011]-, $[0\bar{1}1]$-, and [100]-sliced foils (as illustrated here on the three surfaces of a box). The dislocation density (ρ) of an as-annealed Mo single crystal is estimated to be on the order of 10^6 ~ 10^7 cm^{-2}. According to the Frank-Read dislocation multiplication mechanism [7], dislocation can multiply by repeatedly bowing out a free segment of dislocation line lying in a slip plane, and the shear stress (τ) required to bow out a line segment (l) is given as: $\tau \approx \mu b/l$. Thus, there may exist a critical length ($l^* \approx \mu b/\tau_a$) of free segment for a given applied shear stress (τ_a). Any length of free segment l which is smaller than l^* will be permanently immobile, while length of segment greater than l^* are potentially mobile. Accordingly, an investigation of the relative density (ρ_m/ρ) of mobile dislocation in slip plane is important for studying the yielding behavior of a crystal. An investigation made on this aspect of dislocation configuration is shown in Fig. 2. Here, "in-plane" _[111] near-screw dislocations with a finite segment length in the $\{\bar{1}01\}$ planes are shown in Fig. 2(a). However, there is an uncertainty whether the observed segment is truly a free dislocation segment without any other pinning points such as short jog segments associated with the dislocation line. In other words, there is a difficulty to define free segment length by viewing dislocation from this orientation since it is infeasible to locate the pinning points formed by jog segments along the dislocation line. In fact, the dislocation segment length viewed from the {$\bar{1}01$}-sliced foils may be a measure of the line waviness along the foil normal (or line waviness through thickness). That is, the finite dislocation segment shown in Fig. 2(a) suggests that the dislocation line in the annealed crystals is actually lying across many planes instead of sitting in single crystallographic plane as one usually anticipates. This implies that the initial dislocation structure may contain grown-in jogs of like-sign along a dislocation line and causing the dislocation line to terminate at the free surfaces of thin foil as schematically illustrated in Fig. 2(b).

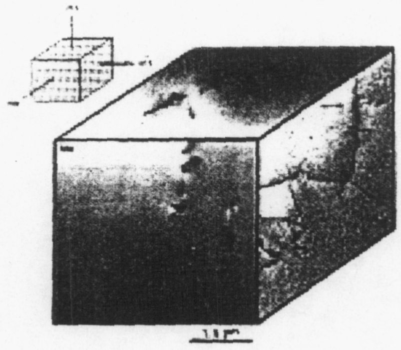

Fig. 1. Initial dislocation structure of an as annealed Mo single crystal.

In fact, the finite length of dislocation segment viewing from the {$\bar{1}01$}-sliced foils may be a measure of the line waviness along the foil normal. This can be visualized readily from a cross-sectional view of _[$\bar{1}\bar{1}1$] screw dislocation shown in Fig. 3(a), in which the screw dislocation in the (011) plane was observed from the foil sliced parallel to the (0$\bar{1}$1) plane. Here, the existence of many long superjogs (50 ~ 100 nm in height) along the _[$\bar{1}\bar{1}1$] screw dislocation line can be seen. In addition, the dislocation line is found to skew away from the [$\bar{1}\bar{1}1$] direction revealing that the dislocation line is also associated with many short superjogs [jog height (d) < 1 nm] or elementary jogs [jog height = interplanar spacing of ($\bar{1}$21) plane = 0.135 nm]. Noted that the height of short superjog or elementary jog is too short to be resolvable using TEM imaging techniques. This examination suggests that the short dislocation segments appeared in the {$\bar{1}01$}-sliced foils is attributed to the formation of jogs along a screw dislocation line which causes it to lie across many {$\bar{1}01$} planes instead of one. Consequently, screw dislocation lines are chopped into short segments in a {$\bar{1}01$}-sliced TEM foils. Similarly, jogged _[111] and _[1$\bar{1}\bar{1}$] screw dislocations were also observed. A jogged _[1$\bar{1}\bar{1}$] screw dislocation viewing from the [0$\bar{1}$1] direction is shown in Fig. 3(b). Here, many large superjogs (50 ~ 100 nm in height) can be readily seen along the dislocation line. Also notice that the lengths of each free segment linked between two superjogs are unequal.

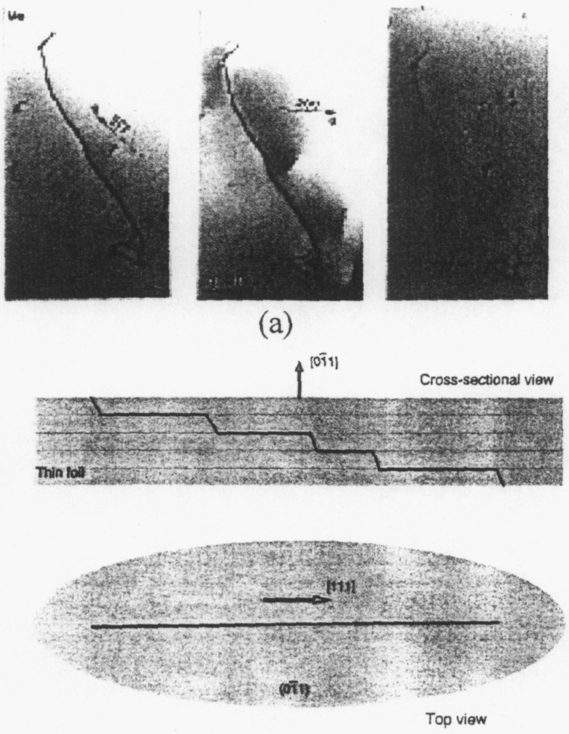

(a)

(b)

Fig. 2. (a) A **g·b** analysis for a ± _ [111] screw dislocation formed in (0$\bar{1}$1)-sliced Mo. (b) Schematic illustrations of cross-sectional and top views of a jogged screw dislocation line within a foil sliced parallel to the slip plane, in which the dislocation line terminates at the free surfaces of thin foil.

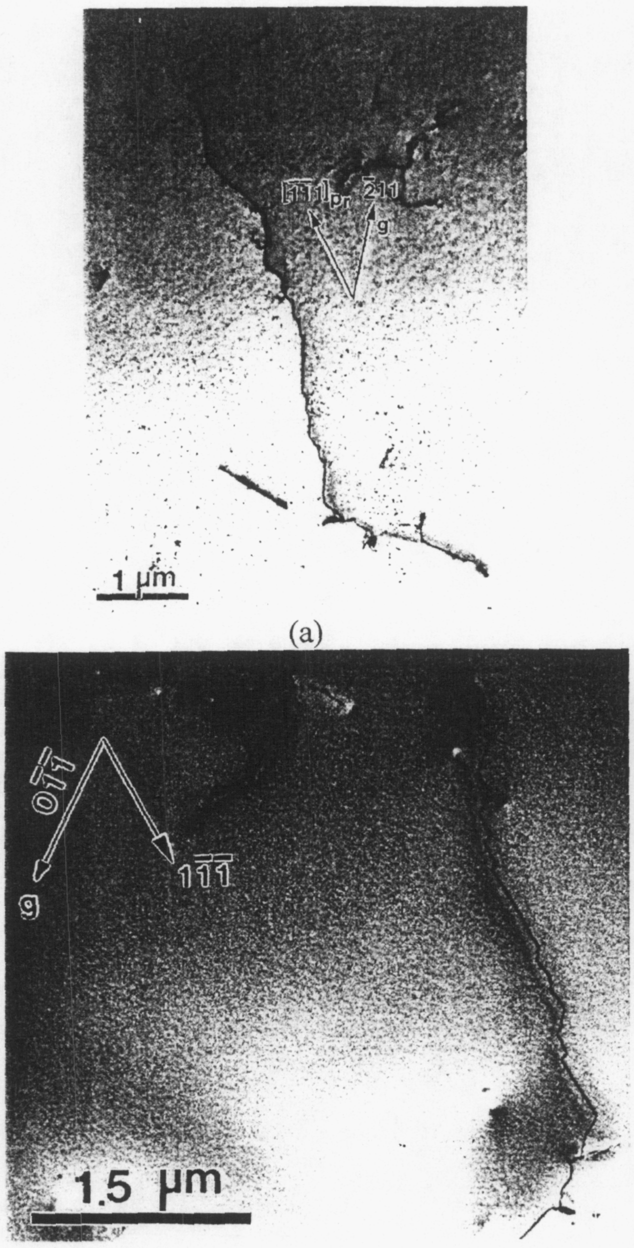

(a)

(b)

Fig 3. TEM images showing (a) a jogged _[ΓΓ1] screw dislocation and (b) a jogged _[1ΓΓ] screw dislocation in as-annealed Mo; viewing direction: [0Γ1].

Deformation substructures

Typical deformation substructures of Mo single crystals compressed for 1 % under strain-rate of 10^{-3} s^{-1} and 1 s^{-1} are shown in Figs. 4(a) and 4(b), respectively. The dislocation density increases about two orders of magnitude to a range of 10^8 ~ 10^9 cm^{-2}. Notice in Fig. 4(a) that many superjogs (marked by arrows) can be seen along screw dislocation lines, and the average jog height, and free segments between superjogs were found to increase significantly as compared to those observed in as-annealed samples (Fig. 3). In general, the screw dislocation lines become straighter and longer comparing to those in as-annealed crystals. However, the formation of dislocation dipoles (debris) as a result of the nonconservative motion of jogged screw dislocations is dependent of the strain rates. While little dislocation dipole (debris) were found in the crystal tested quasi-statically (10^{-3} s^{-1}), more cusps along screw dislocation lines and many dislocation dipoles (debris) were observed in the crystal compressed under the strain rate of 1 s^{-1} as shown in Fig. 4(b).

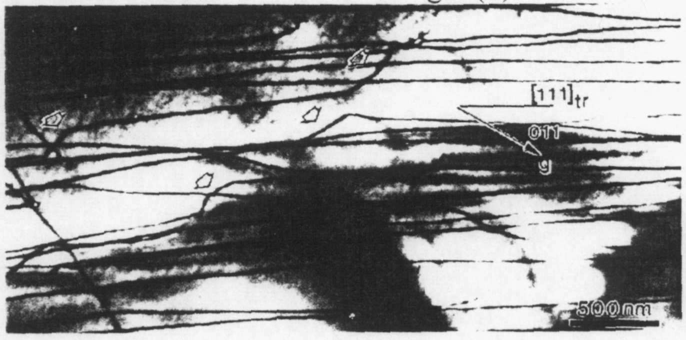

Fig. 4. TEM images showing _[111] screw dislocations associated with superjogs (indicated by arrows) in a crystal compressed for 1% (strain rate: 10^{-3} s^{-1}), viewing direction: [11Γ].

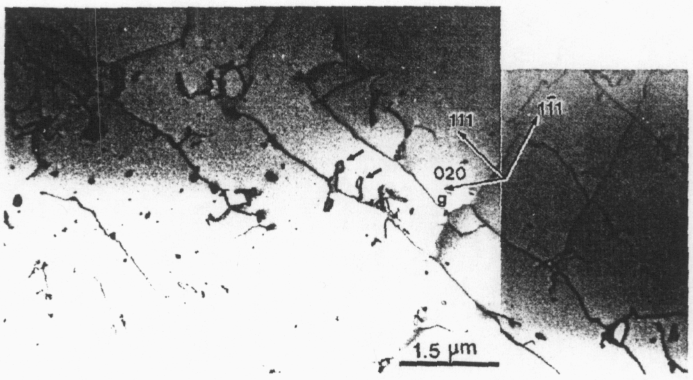

Fig. 5. TEM images showing (a) _[111] screw dislocations associated with dislocation dipoles (indicated by arrows) and many dislocation debris in a crystal compressed for 1% (strain rate: 1 s^{-1}).

Proposed mechanisms for dislocation multiplication and motion

Based upon the results of TEM observations shown above, mechanisms of dislocation multiplication and motion during the early stages of plastic deformation in Mo single crystals under different strain-rate conditions are proposed below. When deformed under a quasi-static condition, the dislocation multiplication is illustrated in Fig. 6. Here, screw dislocation segments (pinned by superjogs) bow out between the superjogs under an applied shear stress (τ) to a certain curvature, yet they are immobile since the initial length (l_o) of each free segment is smaller than a critical length ($l^* \approx \mu b/\tau$) as defined earlier. Beside the force exerted on dislocation segments by the applied shear stress, each superjog is subjected to a net force (F_x) parallel to the Burgers vector due to the bowing of unevenly spaced link segments between jogs under small strains, which is schematically illustrated in Fig. 6(d). The magnitude of net force can be expressed as:

$$F_x = \Gamma(\cos\phi_2 - \cos\phi_1),$$

where $\phi = \sigma bl/2\Gamma$, and Γ is the line tension. Applying Taylor expansion to cosϕ, thus

$$F_x \approx \frac{b^2\sigma^2}{8\Gamma}(l_1^2 - l_2^2).$$

The force causes large loop to grow at the expanse of neighboring short loop by drifting the jog at P. The jog drifting velocity (v_j) can be related to its mobility (D_j/kT) according to the Einstein mobility relation [8, 9]:

$$v_j = \frac{D_j}{kT} F_x$$

where D_j is the jog diffusivity. That is, each jog in Fig. 6(b) moves in such a direction so that the shorter segments ($\overline{CD}$ and $\overline{EF}$) become still shorter and the longer segments ($\overline{AB}$ and $\overline{GH}$) are expanded [10]. The jogs of like-sign tend to coalescence in order to reduced line energy and resulting in the increase of jog height [11]. Consequently, the stress-induced jog pileup and coalescence renders an increase of both segment length and jog height.

Applied shear stress eventually begins to push each line segment between jogs [Fig. 6 (c)] to precede dislocation multiplication when the length (l) of line segments ($\overline{IJ}$ and $\overline{KL}$) and height (d) of superjog ($\overline{JK}$) are greater than critical values defined as following.

$$L > l^* \approx \mu b/\tau, \text{ and}$$

$$d > d_c \approx \mu b/8\pi(1-\nu)\tau.$$

Here, a mutual attraction force between adjacent bowing edge segments of opposite signs can define

d_c. That is, the originally immobile screw dislocations become multiple sources for dislocation multiplication as a result of the process or jog migration and coalescence. This "dynamic" dislocation multiplication source is suggested to be crucial for the dislocation multiplication in the early stage of plastic deformation in Mo.

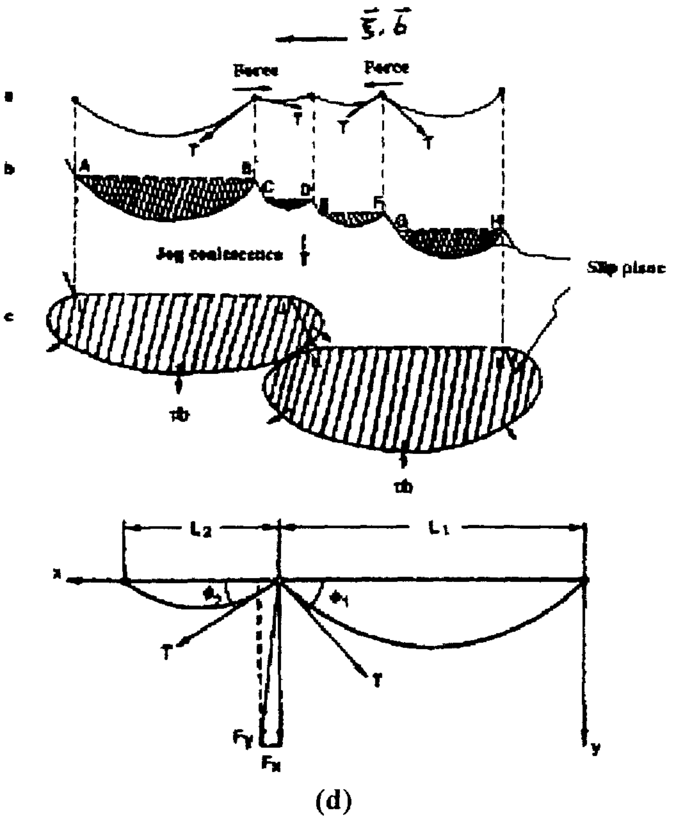

Fig. 6. Schematic illustrations of dislocation multiplication from a jogged screw dislocation. (a) A top view showing dislocation segments pinned by superjogs bowing under stress to a curvature, net forces are generated on jogs due to unbalanced line-tension partials acting on the free segments of unequal lengths. (b) A tilt view of (a) shows the initial heights of like-sign superjogs. (c) Both segment length and jog height increase due to stress-induced jog coalescence. As a result, two multiplication sources are generated at segments $\overline{IJ}$ and $\overline{KL}$. (d) The resolved forces F_x and F_y acting on the jog (pinning point) caused by link segments of unequal lengths, L_1 and L_2 bowing under low strains.

When deformed under a high strain-rate condition, the nucleation and migration of double kinks on screw dislocations become more rapidly according to the following equation [8]:

$$v_k = \frac{\sigma b L D_k}{kT}\exp[-\frac{2W_k}{kT}]$$

where, v_k is the migration velocity of double kinks, L the length of free segment, D_k/kT the kink mobility, D_k the kink diffusivity, W_k the formation energy for double kinks, which is considered to be a function of stress, i.e. it decreases with increasing applied stress. Accordingly, the rapid increase of stress on a link segment causes the double-kinks to pileup at the ends of the segment as shown in Fig. 7 (a). This in turn causes the angle θ *to* increase rapidly to approach 90°, which vanishes the net force on a superjog and thus retards the process for migration and coalescence of superjogs. Under this circumstance, long superjogs may still have sufficiently large jog-height to satisfy the condition for operating the "dynamic" multiplication source. Superjogs of relatively small height, on the other hand, will be unable to meet the condition for multiplication, and the gliding (jogged) screw dislocation will eventually draw out a dislocation dipole as shown in Fig. 7 (b), in which a dislocation dipole consists of two parallel dislocation segments of opposite signs, and are separated from each other by a short distance depending on the jog height (d).

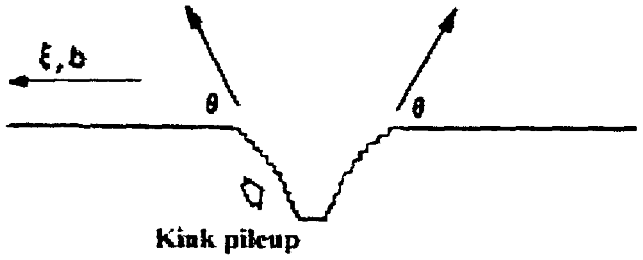

(a)

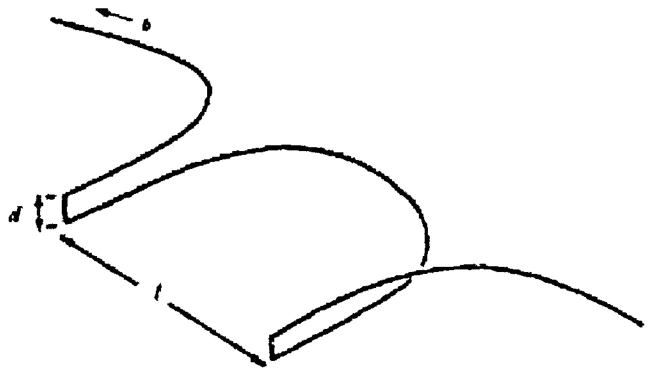

(b)

Fig. 7. Schematic illustrations showing (a) the formation of superkinks as a result of the pileup of kinks at superjog, and (b) two edge dipoles are drawing out from a jogged screw dislocation.

Summary

Initial dislocation structures in as-annealed high-purity Mo single crystals, and deformation substructures of the crystals compressed at room temperature under different strain rates (10^{-3} s^{-1} and 1 s^{-1}) have been examined and studied in order to elucidate the physical mechanisms of dislocation multiplication and motion for dislocation dynamics simulations. It is suggested that the jogged screw dislocations can act as predominant sources for either dislocation multiplication or dipole (debris) formation depending on applied strain rates. When compressed under a quasi-static condition, both the superjog height and length of link segment (between superjogs) can increase by stress-induced jog migration and coalescence, which presumably takes place via the lateral migration (drift) of superjogs driven by unbalanced line-tension partials acting on link segments of unequal lengths. Applied stress begins to push each link segment to precede dislocation multiplication when link length and jog height become greater than critical values. When compressed under a high strain-rate condition, the rapid increase of stress on a link segment causes the nucleation and migration of more double-kinks to pileup at the ends of the segment, which in turn retards the process of jog migration and coalescence. Dislocation dipoles (debris) start to generate as a result of the nonconservative motion of jogged dislocations in which jog heights remain small.

Acknowledgements - This work was performed under the auspices of the U.S. Department of Energy by the University of California, Lawrence Livermore National Laboratory under contract No. W-7405-Eng-48. The authors would like to thank Dr. V. V. Bulatov for providing information regarding Dislocation Dynamics Simulations.

Reference

1. E. Orowan, *Z. Phys.*, **89** (1934), p. 604.
2. M. Polanyi, *Z. Phys.*, **89** (1934), p. 660.
3. G.I. Taylor, *Proc. Roy. Soc.* (London), **A145** (1934), p. 362.
4. L.P. Kubin, G. Canova, M. Condat, B. Devincre, V. Pontikis, and Y. Brechet, *Solid State Phenom.*, **23-24** (1992), p. 455.
5. M. Rhee, H.M. Zbib, J.P. Hirth, H. Huang, and T. Diaz de la Rubia, *Modeling Simul. Mater. Sci. Eng.* **6** (1998), p. 467.
6. K.W. Schwarz and J. Tersoff, *Appl. Phys. Lett*, **69** (1996), p. 1220.
7. F. C. Frank and W. T. Read, in *"Symposium on Plastic Deformation of Crystalline Solids,"* Carnegie Institute of Technology, Pittsburgh, 1950, p. 44.
8. J. P. Hirth and J. Lothe, *"Theory of Dislocations"*, 2nd ed., J. Wiley, New York, 1981.
9. A. Einstein, *"Investigations on the Theory of Brownian Movement,"* Methuen, London (1926), p. 9.
10. J. Weertman and P. Shahinian, *Trans. A.I.M.E.* **209** (1957), p. 1298.
11. N. Louat and C. A. Johnson, *Phil. Mag.* **7** (1962), p. 2051.

From forest hardening to strain hardening in body centered cubic single crystals: simulation and modeling

M. Tang(1), M. Fivel(2), and L. P. Kubin(3)

(1)Physics Directorate, Lawrence Livermore National Laboratory, Livermore, CA 94551
(2)GPM2-CNRS/INPG, BP46, 38402 Saint Martin d'Heres Cedex, France
(3) LEM, CNRS-ONERA, 29, Ave. de la Division Leclerc, BP72, 92322 Chatillon Cedex, France

ABSTRACT:

In body centered cubic (bcc) crystals at low temperature, the thermally activated motion of screw dislocations by the kink pair mechanism governs the yield properties and also affects the strain hardening properties. The strain hardening is studied through two steps, i.e., through forest hardening and dislocation density evolution. The forest hardening has been previously numerically simulated and analyzed by a simple model that applies generally to all bcc metals at low temperature. For the dislocation density evolution, the very first, but crucial, attempt in simulation consists of the development of a boundary condition with dislocation flux balance, which is shown to increase the dislocation density significantly during the early stage of deformation.

Key words: dislocation dynamics; strain hardening; forest hardening; density evolution; dislocation flux; boundary condition

1. Introduction

It is necessary to discern two different regions for the mechanical properties of bcc metals. At high temperatures above the so-called athermal temperature [1][2], the mechanical properties are similar to those typical of face centered cubic (fcc) metals. At low temperatures, due to the complex three-dimensional core structures, screw dislocations exhibit a high intrinsic Peierls barrier and low mobility [2] [3] which govern the flow properties. Then, unlike in fcc metals, dislocation storage and patterning are not effective until large strain [4]. The spatial distribution of dislocations is a random one and the stress-strain curves achieve pseudo-parabolic shapes.

This paper concerns the strain hardening of bcc metals in the low temperature region. Two steps are taken to model the strain hardening. The first one concerns the forest hardening, i.e., the increase of flow stress with respect to the increase of forest dislocation density. Existing knowledge on forest hardening is mostly gained based on fcc crystals, in which the stress increase due to forest interactions is proportional to the square root of the forest dislocation density [5] [6]. For bcc metals at low temperature, the particular core properties of screw dislocations induce a thermally activated mobility (cf. Refs.[2] [3]). A strongly temperature-dependent effective stress, substantially larger than the athermal stress for dislocation junction unzipping, is then needed to move the screw dislocations by the kink pair mechanism. In Section 2, we briefly recall the results obtained on forest hardening using both numerical simulation and rate equation based modeling. The reader is referred to Ref. [2] for details regarding the simulation methodology and to Refs. [7] and [4] for a model of forest hardening derived based on the simulations.

The second step concerns the dislocation density evolution as a function of strain. It is critical to take into account the early stage plastic deformation, i.e., the so-called stage 0, where a large increase in screw dislocation density is expected before the yield stress is reached [1] [2]. This results from the motion of the non-screw components of the initial dislocation density under low applied stresses. This paper presents our first attempt at a quantitative modeling of this density evolution. It consists of developing an improved boundary condition with dislocation flux balance.

Section 3 shows the method for flux-balance, its implementation, and preliminary results to show its effects on stage 0 properties.

2. Forest hardening

The Dislocation Dynamics (DD) simulation of bcc crystals is based on the edge-screw model in a discretized lattice [2][8]. The lattice parameter is typically a few nanometers, thus delimiting a boundary between the elastic properties of the dislocations and core properties. The former is conveniently treated within an elastically isotropic continuum, while the latter are accounted for by introducing local rules in the simulation. The thermally activated motion of screw dislocations is described by an Arrhenius form [9], which is numerically fitted to the yield stress vs. temperature dependence of pure Ta crystals [2]. The edge mobility is treated as infinite and the edge dislocations only stop at equilibrium positions or obstacles.

The typical scenario of a mobile screw segment pinned by attractive obstacles is represented schematically in Fig. 1. Between the obstacles, the dislocation line of length L moves by kink pair nucleation and elementary kink pile-up, forming two curved arms at the junctions. When a critical configuration is reached, measured by the distance X_c traveled by the screw segment, the junctions become mechanically unstable and are destroyed by an unzipping mechanism [10] similar to the one observed in fcc crystals.

>From Fig. 1, two mechanisms of strain hardening can be deduced. First, the free-length L is decreased by an increase of obstacle density. Thus the velocity of the screw is decreased due to reduced kink pair nucleation probability along the line. This must be compensated by an increase of

effective stress under constant strain rate condition. Second, the line tension coming from the curved non-screw part always tends to slow down the mobile screw segment. After a few steps of derivation combining these two effects, the total hardening can be expressed as (see Ref. [7] for details)

$$\frac{\Delta\tau}{\mu}=\frac{S_0}{\mu}\ln\left(\frac{\rho_f}{\rho_{f0}}\right)+K\rho_f \qquad (1)$$

where μ is the shear modulus, ρ_{fo} is a scaling density, S_o is the strain rate sensitivity and K another strain rate and temperature dependent quantity. We see that forest hardening in bcc metals at low temperature is due to two contributions: i) - A logarithmic term, which stems from the proportionality of the screw segment velocities to their lengths. This free-length effect has been discussed by Louchet et al. [11]. ii) - A practically linear line tension contribution, similar to the one considered by Rauch [12]. In addition, the forest hardening in bcc metals strongly depends on both strain rate and temperature. With increasing temperature or for very high dislocation densities, this expression progressively merges into the classical square root relationship found in fcc-like materials. This model was originally derived from a simulation work that is not recalled here (cf. Ref. [7]). It fairly well reproduces the numerical results as well as the few available data, confirming that forest hardening in bcc metals at low temperature is not proportional to the square root of the dislocation density, except at large strains.

3. Dislocation flux balance

So far, we have discussed forest hardening rather than strain hardening. To complete the model, knowledge of the strain dependence of the forest dislocation density is needed, which is non-trivial for bcc crystals. The major problem stems from the occurrence of an exhaustion stage (stage 0) during the early pseudo-elastic loading of the specimen. During this stage, the non-screw segments initially present in the microstructure can move over long distances at relatively low stress levels, producing dipoles of elongated immobile screw segments essentially on all slip systems [1] [2]. As a consequence, the density of screws, hence the forest density, at yield stress can be orders of magnitude larger than the initial one. Stage 0 is extended further as the temperature is lower and the strain rate is higher.

While the stage 0 density evolution is undoubtedly difficult to model, it is also non-trivial to simulate. Due to their large mobility, the edge dislocations have long mean free paths that lead to significant loss of edge segments from the simulation box and make the typical simulation box sizes (a few tens of micrometers) too small to be representative for a bulk material. Even though junction formation can momentarily stop the edges, the junctions are easily unzipped due to fast increase of flow stress during stage 0 and edges will leave out of the simulation box eventually.

3.1. Flux-balanced boundary condition

The solution lies in the boundary condition. Currently, all existing dislocation dynamics simulations aimed for bulk simulations do not account of the dislocation segments that disappear from the simulation box boundaries. Our simulations use the so-called quasi-free surface boundary condition [13]. The simulations are performed with all segments inside the simulation box and the mechanical properties such as density and strain are only calculated within a sphere located inside the simulated volume. For fcc crystals, this allows to avoid dealing with a region close to the surfaces where the density is depleted. However, for bcc crystals, due to the long mean free path of edges and long length of screw segments, the sphere method was found to be ineffective.

Recently, a rigorous mathematical formulation of the boundary value problem of dislocation dynamics was developed by A. El-Azab [14]. For the case where the simulated volume is a representative sub-volume embedded inside a larger bulk material, an important boundary condition was derived to deal with dislocation fluxes across the boundaries of the simulated volume. It requires that the net dislocation flux should be identically zero on the surfaces, i.e., $\vec{v}\phi^j\big|_{in} = \vec{v}\phi^j\big|_{out}$ (see Ref. [14] for details). Here, ϕ^j is a scalar line density on slip system j corresponding to velocity $\vec{v}$. The direction of the velocity with respect to the positive normal to the surface determines whether the flux is inward or outward. One can show easily that the dislocation flux $\vec{v}\phi$ is equivalent to the rate of swept slip-area per unit volume or shear strain [14]. The latter can be conveniently monitored in the simulation and is used as a criterion for flux balance. In a discrete DD simulation, the flux balance condition per unit time is reduced to

$$A^j_{net} = \sum_i A^j_i = 0, \quad j = 1, 2 \ldots \text{all slip systems} \tag{2}$$

where A^j_{net} is the total net swept slip-area for slip system j and A^j_i is the swept area across the boundaries due to the movement of ith segment on slip system j. Fig. 2 shows schematically a few typical configurations of segments across the surfaces. The total net flux is always positive (i.e., outward) without flux balance. Thus, proper procedure to introduce inward flux is needed.

The inward flux is introduced in such a way that it consists of half-loops ending at the surfaces, as illustrated by Fig. 2(e). Each half-loop consists of one edge and two screw segments. The lengths of all three segments are made stress dependent. The edge length is calculated by $L_e = \alpha\mu b/\tau_a$, where τ_a is the applied stress and α is a line tension coefficient. The sign of the Burgers vector is chosen so that the configuration will move inside the simulation box under the applied stress. During the first simulation steps, the line tension coefficient α is artificially enhanced by a small amount so that the generated half-loops may enter the simulation volume following immediate increase of flow stress. The location of the half-loops at the surface is chosen randomly with one condition that the coordinates of the segments must be consistent with the underlying discrete lattice of the simulation. Once generated, one single half-loop contributes an inward flux of δA to the net flux of its slip system and a shear strain of $b\delta A/V$ to the total strain of its slip system, where $\delta A = \frac{1}{2}L_e(L_s^1 + L_s^2)$ and L_s^1 and L_s^2 are the lengths of the two screw segments. The flux balance is performed for each slip system and during the whole course of simulation whenever the accumulated net flux allows one or more half-loops to be introduced.

3.2. Results of dislocation flux balance

Simulations are then performed to test the above procedure for flux balance. Two simplified simulations are chosen with the exact same conditions (cf. Fig. 3 for details), except that only one is implemented with flux balance. Fig. 3 shows the stress-strain curves and total densities. The arrows mark the end of stage 0 or the beginning of the macro-yield, where the screw dislocations start to move and multiply. As expected, the flux balance has extended the stage 0 strain from $4.25\text{x}10^{-5}$ to $6.05\text{x}10^{-5}$. The density at the end of stage 0 has increased from $1.8\text{x}10^{11}/\text{m}^2$ to $4.0\text{x}10^{11}/\text{m}^2$ with flux balance. Note that the flow stress with flux balance in Fig. 3(a) is slightly lower than the one without flux balance. This is because the mobile densities enter through a pre-factor into the Arrhenius rate equation [2]. Fig. 4(a) shows the detailed information about the net flux and the number of half-loops introduced. The net accumulated swept slip-area with flux balance is essentially maintained to be zero. Without flux balance, the net flux increases rapidly at the beginning of plastic deformation signaling large outward flux due to loss of edge segments from the simulation box. At some point, the saturation is reached. This is because most edge segments reach their critical bow-out configuration and move by large distances at low flow stress levels at the beginning of the deformation. Once the initial edges have moved out from the simulation box, the screws are essentially immobile and no further slip activity occurs until the macro-yield point when the screw segments start to move. Correspondingly, the number of half-loops as shown in Fig. 4(b) are mostly introduced during the early stage of deformation when the outward flux is large. These last features are, however, direct consequence of the implementation scheme. As discussed below, a simple additional rule is needed to obtain a fully realistic picture of stage 0.

4. Summary and conclusions

The forest hardening in bcc metals at low temperature has shown characteristic different behavior than that of fcc metals in terms of its dependence on the forest density and its strong coupling to temperature and strain rate. However, a quantitative experimental check of the flow stress vs. forest density relation for bcc metals at low temperature is not yet available due to lack of density measurements. The flux-balanced boundary condition has shown sizable effect in increasing the dislocation density during stage 0. While an essential step has been taken to implement the flux balance, the current implementation is not satisfactory since it does not take into consideration a physical time scale that controls the inward flux balance. In addition, the mean-free path of the edge segments being usually larger than the linear dimension of the simulated volume, one has to consider the possibility of an edge density continuously entering and leaving the simulation box without affecting the flux balance condition. As a result, the stage 0 strain and the increase of dislocation densities are at present significantly underestimated compared to those in a real bcc crystal of high purity. Further development is in progress that is expected to bring the stage 0 deformation to about 0.1% for a typical initial dislocation density ($\sim 10^{11} / \mathrm{m}^2$). Then, simulations will be performed to quantify the density evolution as a function of strain. Combined with the forest model, this will provide a general description of strain hardening in bcc metals at low temperature.

Acknowledgements

We acknowledge discussions with Dr. A. El-Azab. The work of M. Tang was performed under the auspices of the U.S. Department of Energy by the University of California Lawrence Livermore National Laboratory under contract number W-7405-ENG-48. The computation facility is in part supported by the DoD High Performance Computing Modernization program at the Aeronautical Systems Center Major Shared Research Center (ASC/MSRC).

Figure Captions

Figure 1. Schematic drawing of the configuration of a screw dislocation line pinned by strong forest obstacles. The initial straight line reaches a critical configuration after a moving distance of X_c, which corresponds to a critical angle θ_c.

Figure 2. Schematic drawing of segments gliding in a (110) slip plane and leaving the boundaries of the simulated volume. The shaded areas are examples of the areas A_i^j in Eqn. 2 (positive for outward flux; negative for inward flux). In (a) and (b), an edge segment moves outwards; in (c), a screw segment moves outwards; in (d), a screw segment moves inwards; in (e), a half-loop with area δA is introduced. The directions of screw (<111>) and edge (<112>) segments are indicated.

Figure 3. Stress-strain curves (a) and total dislocation densities (b) obtained from two simulations performed at T= 77 K, with a strain rate of $10^{-5}/s$, under an uniaxial loading orientation <100>. The simulation box size is $15\mu m$. The initial dislocation density is $0.5x10^{11}/m^2$. It consists of edge segments in the slip system $<111>(10\bar{1})$ with an average length of $1/\sqrt{\rho} = 4.47\mu m$ and with a triangular length distribution peaked at $1.47\mu m$. The solid and dashed lines are with and without flux balance respectively.

Figure 4. (a) - The accumulated net flux (in arbitrary units) as a function of time with (solid lines) and without (dashed lines) flux balance. (b) - The number of half-loops introduced with flux balance.

References

[1] L. P. Kubin, Rev. Deform. Behav. Mater. 1 (1976) 244.

[2] M. Tang, L. P. Kubin, G. R. Canova, Acta mater. 9 (1998) 3221.

[3] M. S. Duesbery, V. Vitek, Acta mater. 46 (1998) 1481.

[4] L. P. Kubin, B. Devincre, From dislocation mechanisms to dislocation microstructures and strain hardening, J. B. Bilde-Sorensen, et al., Eds., *20th Riso International Sympsoium on Materials Science*, Riso National Laboratory, Roskilde, Denmark (1999), pp. 61-83.

[5] J. G. Sevillano, in *Materials Science and Technology* H. Mughrabi, Ed. (Weinheim:VCH, 1993), vol. 6, pp. 19-88.

[6] B. Devincre, L. P. Kubin, Modelling Simul. Mater. Sci. Eng. 2 (1994) 559.

[7] M. Tang, B. Devincre, L. P. Kubin, Modelling Simul. Mater. Sci. Eng. 7 (1999) 893.

[8] L. P. Kubin, et al., Solid State Phenom. 23-24 (1992) 455.

[9] U. F. Kocks, A. S. Argon, M. F. Ashby, *Thermodynamics and kinetics of slip*. B. Chalmers, J. W. Christian, T. B. Massalski, Eds., Progress in Materials Science (Pergamon, Oxford, 1975), vol. 19.

[10] L. P. Kubin, B. Devincre, M. Tang, J. Comput.-Aided Mater. Design 5 (1998) 31.

[11] F. Louchet, L. P. Kubin, D. Vesely, Phil. Mag. A. 39 (1979) 433.

[12] E. F. Rauch, Key Eng. Mater. 97-98 (1994) 371.

[13] M. C. Fivel, G. R. Canova, Modelling Simul. Mater. Sci. Eng. 7 (1999) 753.

[14] A. El-Azab, Modelling Simul. Mater. Sci. Eng. 8 (2000) 37.

INITIAL DISLOCATION STRUCTURE AND DYNAMIC DISLOCATION MULTIPLICATION IN Mo SINGLE CRYSTALS

L. M. Hsiung and D. H. Lassila
Lawrence Livermore National Laboratory
Chemistry and Materials Science Directorate
L-352, P.O. Box 808
Livermore, CA 94551-9900

Abstract

Initial dislocation structures in as-annealed high-purity Mo single crystals, and deformation substructures of the crystals compressed at room temperature under different strain rates have been examined and studied in order to elucidate the physical mechanisms of dislocation multiplication and motion in the early stages of plastic deformation. The initial dislocation density was measured to be in a range of $10^6 \sim 10^7$ cm^{-2}. More importantly numerous grown-in superjogs were observed along screw dislocation lines. After testing in compression, dislocation density (mainly screw dislocations) increased to $10^7 \sim 10^8$ cm^{-2}. Besides, the formation of dislocation dipoles (debris) due to the nonconservative motion of jogged screw dislocations was found to be dependent of the strain rates. While little dislocation dipoles (debris) were found in the crystal tested quasi-statically (10^{-3} s^{-1}), more cusps along screw dislocation lines and numerous dislocation dipoles (debris) were observed in the crystal compressed under the strain rate of 1 s^{-1}. Physical mechanisms for dislocation multiplication as well as dipole formation from jogged screw dislocations under different strain rate conditions are accordingly proposed and discussed.

Introduction

Since the initial discovery of dislocations in 1934 [1-3], it has been realized that crystal plasticity properties are derivable, at least in principle, from the aggregate behavior of dislocations. However, a quantitative connection between dislocation theory and the phenomenology of crystal plasticity is yet to be established owing to the immense computational complexity of the task for dealing with a large number of dislocations and the multitude of their physical behaviors. Starting in the early 90's [4], the realization that bigger and faster computers may be used for crystal plasticity simulations has led to the development of a powerful computational methodology for dislocation dynamics (DD). The predictive power of the various DD implementations available today is based on their ability to incorporate, in a computationally tractable manner, multiple and complex mechanisms of dislocation behavior. While the current trend in DD simulations is to let dislocations behave most naturally [5,6], computational limitations often dictate that simplified rules for dislocation unit processes to be adopted [4]. One of the key uncertainties in the DD simulations is how dislocations multiply and move during plastic deformation. To date, several dislocation multiplication mechanisms have been proposed in literature. Typically, dislocation multiplication is considered to take place when a dislocation attains a certain configuration. For example, the well-known Frank-Read (FR) source [7] requires a configuration that both ends of a mobile dislocation segment be pinned (constrained) at two points as a result of either dislocation network or dislocation bend. However, because of an ill-defined nature of pinning points for dislocation multiplication, dislocation sources are usually introduced in the DD simulations in a presumption or an ad hoc manner by setting up a constrained dislocation configuration, which is most often unrealistic. For instance, the initial dislocation configuration for an FR multiplication source may be simply given as a dislocation segment linked between two pinning points with an arbitrarily given length, and dislocation multiplication may thus be mimic or simulated according to the FR multiplication mechanism.

In order to make the DD simulations for dislocation multiplication more realistic, there is a need to understand the correlation between initial dislocation structures (dislocation density, dislocation configuration, free dislocation link length, and grown-in jogs...) and dislocation multiplication during plastic deformation. Accordingly, the main purpose of this investigation is to examine and compare the initial dislocation structures of annealed (high-purity) Mo crystals, and deformation substructures of slightly compressed Mo crystals in order to elucidate the underlying mechanisms of dislocation multiplication and motion during early stages of plastic deformation. Since numerous grown-in superjogs have been observed along dislocation lines within as-annealed Mo crystals, emphasis has been placed upon the strain-rate effect of kink-jog interactions on the dislocation multiplication and motion in the early stages of plastic deformation in Mo single crystals. A preliminary result is reported here.

Experimental

Since the Mo single crystals used for dislocation dynamics experiment must have high purity and low dislocation density in order to establish initial conditions for subsequent dislocation dynamics simulations, the high-purity Mo single crystals were fabricated using a standard electron-beam melting process by Accumet Materials Company, Ossining, NY. The interstitial impurities (ppm in weight) in the as-fabricated crystals are O: 25; N: <10; H: <5; C: <10, respectively. Prior to compression test, the test samples were heat treated at 1500° C for 1 h, 1200° C for 1 h, and 1000° C for 1 h at a vacuum of 8 x 10^{-11} Torr. Testing of Mo single crystals involves compressing the test samples between two platen surfaces under precise conditions. To measure shear strain during compression, a 3-element rosette gage was bonded in the gage section on each side of the sample. Compression tests were performed on test samples with [118] and $[\bar{2}\ 9\ 20]$ compression axes. These two orientations were originally chosen to investigate deformation behavior associated with the $(\bar{1}\bar{1}2)[111]$ and $(\bar{1}01)[111]$ slip systems, respectively. The samples were compressed at a normal strain rate of 10^{-3} s^{-1} for the [118]-oriented sample, and 1 s^{-1} for the $[\bar{2}\ 9\ 20]$-oriented sample, and both samples were compressed to a value of ~1% axial strain. TEM foils were sliced from the gage section of the tested piece with the foil sliced parallel to the $(\bar{1}\bar{1}2)$ plane from [118]-oriented sample, and the $(\bar{1}01)$ plane for the $[\bar{2}\ 9\ 20]$-oriented sample. TEM specimens were finally prepared by a standard twinjet electropolishing technique in a solution of 75 vol.% ethanol and 25 vol.% sulfuric acid at ~25 V and -10° C.

Results and Discussion

Initial dislocation structures

Figure 1 shows the initial dislocation structures observed from the [011]-, $[0\bar{1}1]$-, and [100]-sliced foils (as illustrated here on the three surfaces of a box). The dislocation density (ρ) of an as-annealed Mo single crystal is estimated to be on the order of 10^6 ~ 10^7 cm^{-2}. According to the Frank-Read dislocation multiplication mechanism [7], dislocation can multiply by repeatedly bowing out a free segment of dislocation line lying in a slip plane, and the shear stress (τ) required to bow out a line segment (l) is given as: $\tau \approx \mu b/l$. Thus, there may exist a critical length ($l^* \approx \mu b/\tau_a$) of free segment for a given applied shear stress (τ_a). Any length of free segment l which is smaller than l^* will be permanently immobile, while length of segment greater than l^* are potentially mobile. Accordingly, an investigation of the relative density (ρ_m/ρ) of mobile dislocation in slip plane is important for studying the yielding behavior of a crystal. An investigation made on this aspect of dislocation configuration is shown in Fig. 2. Here, "in-plane" _[111] near-screw dislocations with a finite segment length in the $\{\bar{1}01\}$ planes are shown in Fig. 2(a). However, there is an uncertainty whether the observed segment is truly a free dislocation segment without any other pinning points such as short jog segments associated with the dislocation line. In other words, there is a difficulty to define free segment length by viewing dislocation from this orientation since it is infeasible to locate the pinning points formed by jog segments along the dislocation line. In fact, the dislocation segment length viewed from the {$\bar{1}$01}-sliced foils may be a measure of the line waviness along the foil normal (or line waviness through thickness). That is, the finite dislocation segment shown in Fig. 2(a) suggests that the dislocation line in the annealed crystals is actually lying across many planes instead of sitting in single crystallographic plane as one usually anticipates. This implies that the initial dislocation structure may contain grown-in jogs of like-sign along a dislocation line and causing the dislocation line to terminate at the free surfaces of thin foil as schematically illustrated in Fig. 2(b).

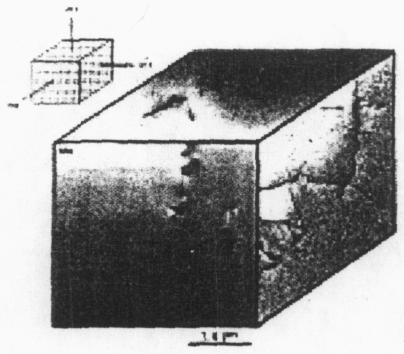

Fig. 1. Initial dislocation structure of an as annealed Mo single crystal.

In fact, the finite length of dislocation segment viewing from the {$\bar{1}$01}-sliced foils may be a measure of the line waviness along the foil normal. This can be visualized readily from a cross-sectional view of _[$\bar{1}\bar{1}$1] screw dislocation shown in Fig. 3(a), in which the screw dislocation in the (011) plane was observed from the foil sliced parallel to the (0$\bar{1}$1) plane. Here, the existence of many long superjogs (50 ~ 100 nm in height) along the _[$\bar{1}\bar{1}$1] screw dislocation line can be seen. In addition, the dislocation line is found to skew away from the [$\bar{1}\bar{1}$1] direction revealing that the dislocation line is also associated with many short superjogs [jog height (d) < 1 nm] or elementary jogs [jog height = interplanar spacing of ($\bar{1}$21) plane = 0.135 nm]. Noted that the height of short superjog or elementary jog is too short to be resolvable using TEM imaging techniques. This examination suggests that the short dislocation segments appeared in the {$\bar{1}$01}-sliced foils is attributed to the formation of jogs along a screw dislocation line which causes it to lie across many {$\bar{1}$01} planes instead of one. Consequently, screw dislocation lines are chopped into short segments in a {$\bar{1}$01}-sliced TEM foils. Similarly, jogged _[111] and _[1$\bar{1}\bar{1}$] screw dislocations were also observed. A jogged _[1$\bar{1}\bar{1}$] screw dislocation viewing from the [0$\bar{1}$1] direction is shown in Fig. 3(b). Here, many large superjogs (50 ~ 100 nm in height) can be readily seen along the dislocation line. Also notice that the lengths of each free segment linked between two superjogs are unequal.

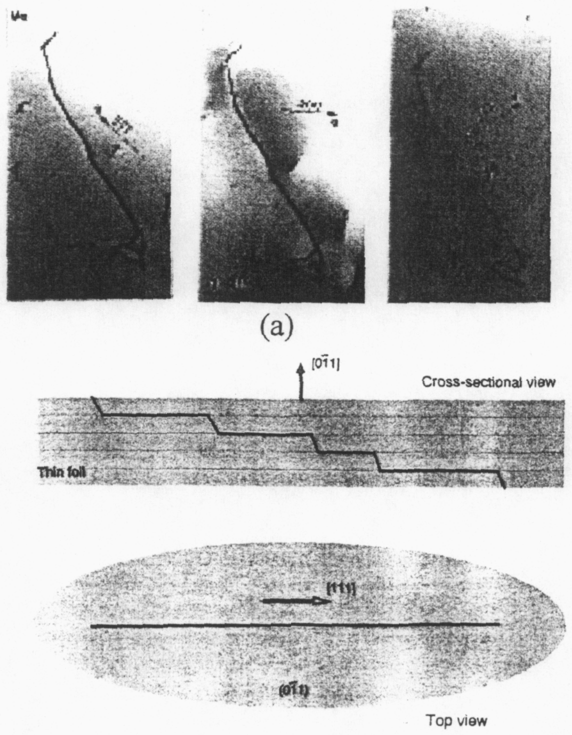

(a)

(b)

Fig. 2. (a) A **g·b** analysis for a ± _ [111] screw dislocation formed in (0$\bar{1}$1)-sliced Mo. (b) Schematic illustrations of cross-sectional and top views of a jogged screw dislocation line within a foil sliced parallel to the slip plane, in which the dislocation line terminates at the free surfaces of thin foil.

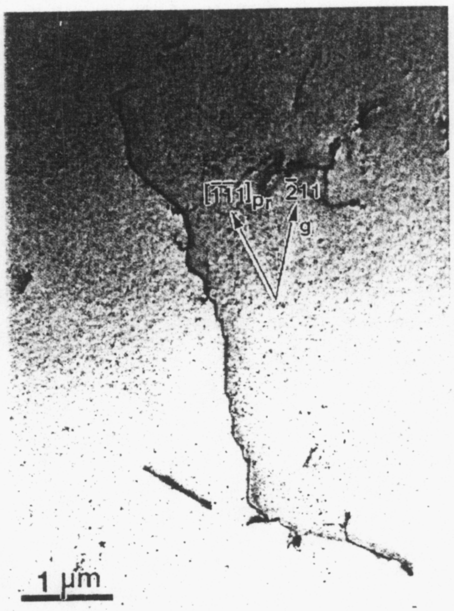

(a)

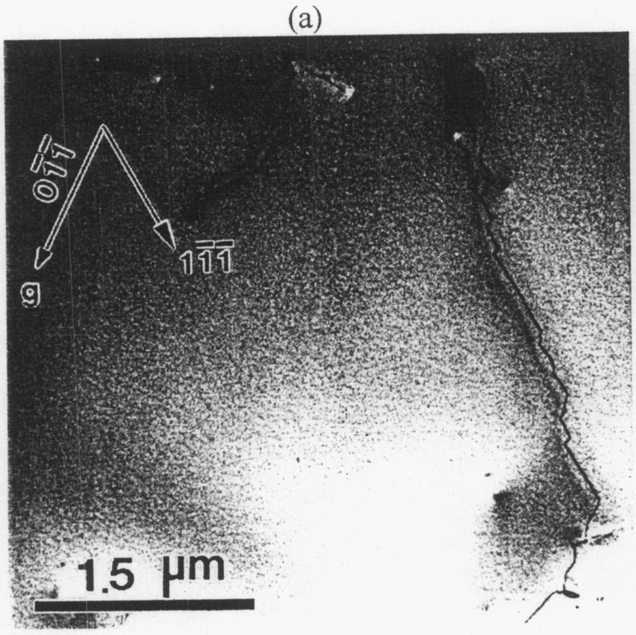

(b)

Fig 3. TEM images showing (a) a jogged _[ΓΓ1] screw dislocation and (b) a jogged _[1ΓΓ] screw dislocation in as-annealed Mo; viewing direction: [0Γ1].

Deformation substructures

Typical deformation substructures of Mo single crystals compressed for 1 % under strain-rate of 10^{-3} s^{-1} and 1 s^{-1} are shown in Figs. 4(a) and 4(b), respectively. The dislocation density increases about two orders of magnitude to a range of 10^8 ~ 10^9 cm^{-2}. Notice in Fig. 4(a) that many superjogs (marked by arrows) can be seen along screw dislocation lines, and the average jog height, and free segments between superjogs were found to increase significantly as compared to those observed in as-annealed samples (Fig. 3). In general, the screw dislocation lines become straighter and longer comparing to those in as-annealed crystals. However, the formation of dislocation dipoles (debris) as a result of the nonconservative motion of jogged screw dislocations is dependent of the strain rates. While little dislocation dipole (debris) were found in the crystal tested quasi-statically (10^{-3} s^{-1}), more cusps along screw dislocation lines and many dislocation dipoles (debris) were observed in the crystal compressed under the strain rate of 1 s^{-1} as shown in Fig. 4(b).

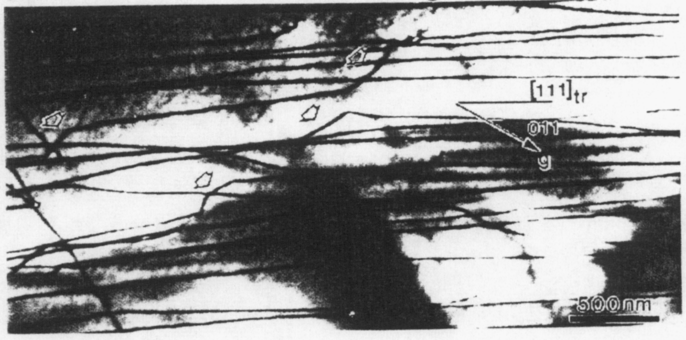

Fig. 4. TEM images showing _[111] screw dislocations associated with superjogs (indicated by arrows) in a crystal compressed for 1% (strain rate: 10^{-3} s^{-1}), viewing direction: [11Γ].

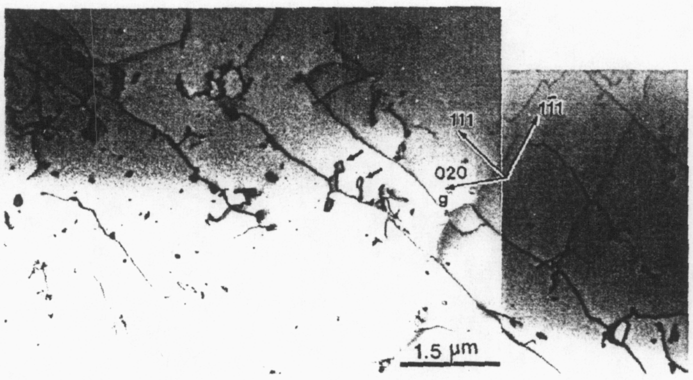

Fig. 5. TEM images showing (a) _[111] screw dislocations associated with dislocation dipoles (indicated by arrows) and many dislocation debris in a crystal compressed for 1% (strain rate: 1 s^{-1}).

Proposed mechanisms for dislocation multiplication and motion

Based upon the results of TEM observations shown above, mechanisms of dislocation multiplication and motion during the early stages of plastic deformation in Mo single crystals under different strain-rate conditions are proposed below. When deformed under a quasi-static condition, the dislocation multiplication is illustrated in Fig. 6. Here, screw dislocation segments (pinned by superjogs) bow out between the superjogs under an applied shear stress (τ) to a certain curvature, yet they are immobile since the initial length (l_o) of each free segment is smaller than a critical length ($l^* \approx \mu b/\tau$) as defined earlier. Beside the force exerted on dislocation segments by the applied shear stress, each superjog is subjected to a net force (F_x) parallel to the Burgers vector due to the bowing of unevenly spaced link segments between jogs under small strains, which is schematically illustrated in Fig. 6(d). The magnitude of net force can be expressed as:

$$F_x = \Gamma(\cos\phi_2 - \cos\phi_1),$$

where $\phi = \sigma bl/2\Gamma$, and Γ is the line tension. Applying Taylor expansion to $\cos\phi$, thus

$$F_x \approx \frac{b^2\sigma^2}{8\Gamma}(l_1^2 - l_2^2).$$

The force causes large loop to grow at the expanse of neighboring short loop by drifting the jog at P. The jog drifting velocity (v_j) can be related to its mobility (D_j/kT) according to the Einstein mobility relation [8, 9]:

$$v_j = \frac{D_j}{kT}F_x$$

where D_j is the jog diffusivity. That is, each jog in Fig. 6(b) moves in such a direction so that the shorter segments ($\overline{CD}$ and $\overline{EF}$) become still shorter and the longer segments ($\overline{AB}$ and $\overline{GH}$) are expanded [10]. The jogs of like-sign tend to coalescence in order to reduced line energy and resulting in the increase of jog height [11]. Consequently, the stress-induced jog pileup and coalescence renders an increase of both segment length and jog height.

Applied shear stress eventually begins to push each line segment between jogs [Fig. 6 (c)] to precede dislocation multiplication when the length (l) of line segments ($\overline{IJ}$ and $\overline{KL}$) and height (d) of superjog ($\overline{JK}$) are greater than critical values defined as following.

$$L > l^* \approx \mu b/\tau, \text{ and}$$

$$d > d_c \approx \mu b/8\pi(1-\nu)\tau.$$

Here, a mutual attraction force between adjacent bowing edge segments of opposite signs can define

d_c. That is, the originally immobile screw dislocations become multiple sources for dislocation multiplication as a result of the process or jog migration and coalescence. This "dynamic" dislocation multiplication source is suggested to be crucial for the dislocation multiplication in the early stage of plastic deformation in Mo.

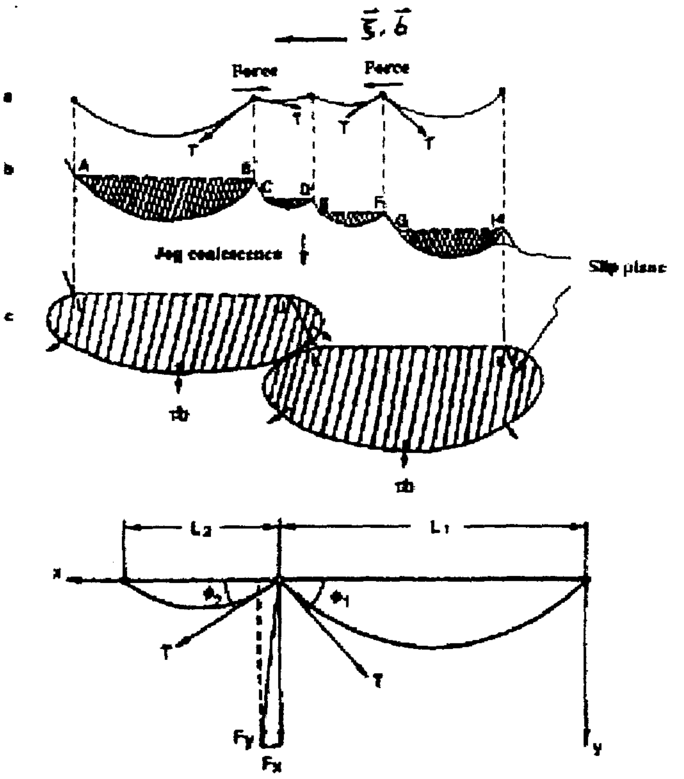

(d)

Fig. 6. Schematic illustrations of dislocation multiplication from a jogged screw dislocation. (a) A top view showing dislocation segments pinned by superjogs bowing under stress to a curvature, net forces are generated on jogs due to unbalanced line-tension partials acting on the free segments of unequal lengths. (b) A tilt view of (a) shows the initial heights of like-sign superjogs. (c) Both segment length and jog height increase due to stress-induced jog coalescence. As a result, two multiplication sources are generated at segments $\overline{IJ}$ and $\overline{KL}$. (d) The resolved forces F_x and F_y acting on the jog (pinning point) caused by link segments of unequal lengths, L_1 and L_2 bowing under low strains.

When deformed under a high strain-rate condition, the nucleation and migration of double kinks on screw dislocations become more rapidly according to the following equation [8]:

$$v_k = \frac{\sigma b L D_k}{kT}\exp\left[-\frac{2W_k}{kT}\right]$$

where, v_k is the migration velocity of double kinks, L the length of free segment, D_k/kT the kink mobility, D_k the kink diffusivity, W_k the formation energy for double kinks, which is considered to be a function of stress, i.e. it decreases with increasing applied stress. Accordingly, the rapid increase of stress on a link segment causes the double-kinks to pileup at the ends of the segment as shown in Fig. 7 (a). This in turn causes the angle θ *to* increase rapidly to approach 90°, which vanishes the net force on a superjog and thus retards the process for migration and coalescence of superjogs. Under this circumstance, long superjogs may still have sufficiently large jog-height to satisfy the condition for operating the "dynamic" multiplication source. Superjogs of relatively small height, on the other hand, will be unable to meet the condition for multiplication, and the gliding (jogged) screw dislocation will eventually draw out a dislocation dipole as shown in Fig. 7 (b), in which a dislocation dipole consists of two parallel dislocation segments of opposite signs, and are separated from each other by a short distance depending on the jog height (d).

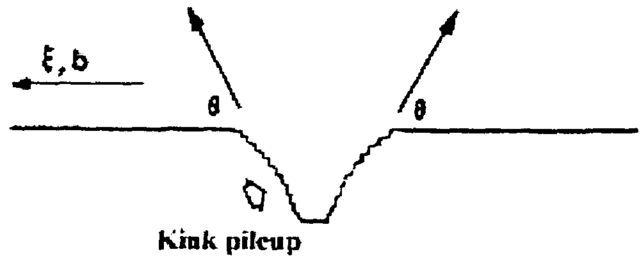

(a)

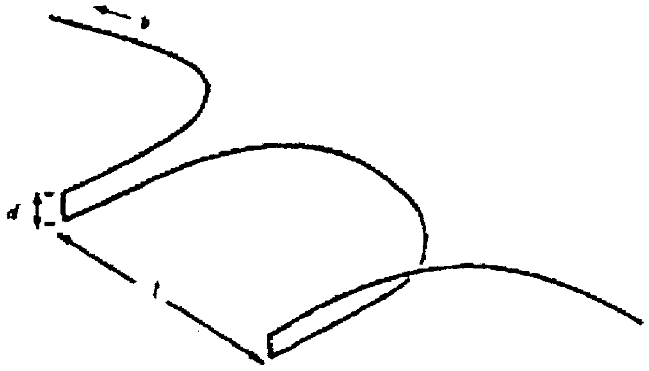

(b)

Fig. 7. Schematic illustrations showing (a) the formation of superkinks as a result of the pileup of kinks at superjog, and (b) two edge dipoles are drawing out from a jogged screw dislocation.

Summary

Initial dislocation structures in as-annealed high-purity Mo single crystals, and deformation substructures of the crystals compressed at room temperature under different strain rates (10^{-3} s^{-1} and 1 s^{-1}) have been examined and studied in order to elucidate the physical mechanisms of dislocation multiplication and motion for dislocation dynamics simulations. It is suggested that the jogged screw dislocations can act as predominant sources for either dislocation multiplication or dipole (debris) formation depending on applied strain rates. When compressed under a quasi-static condition, both the superjog height and length of link segment (between superjogs) can increase by stress-induced jog migration and coalescence, which presumably takes place via the lateral migration (drift) of superjogs driven by unbalanced line-tension partials acting on link segments of unequal lengths. Applied stress begins to push each link segment to precede dislocation multiplication when link length and jog height become greater than critical values. When compressed under a high strain-rate condition, the rapid increase of stress on a link segment causes the nucleation and migration of more double-kinks to pileup at the ends of the segment, which in turn retards the process of jog migration and coalescence. Dislocation dipoles (debris) start to generate as a result of the nonconservative motion of jogged dislocations in which jog heights remain small.

Acknowledgements - This work was performed under the auspices of the U.S. Department of Energy by the University of California, Lawrence Livermore National Laboratory under contract No. W-7405-Eng-48. The authors would like to thank Dr. V. V. Bulatov for providing information regarding Dislocation Dynamics Simulations.

Reference

1. E. Orowan, *Z. Phys.*, **89** (1934), p. 604.
2. M. Polanyi, *Z. Phys.*, **89** (1934), p. 660.
3. G.I. Taylor, *Proc. Roy. Soc.* (London), **A145** (1934), p. 362.
4. L.P. Kubin, G. Canova, M. Condat, B. Devincre, V. Pontikis, and Y. Brechet, *Solid State Phenom.*, **23-24** (1992), p. 455.
5. M. Rhee, H.M. Zbib, J.P. Hirth, H. Huang, and T. Diaz de la Rubia, *Modeling Simul. Mater. Sci. Eng.* **6** (1998), p. 467.
6. K.W. Schwarz and J. Tersoff, *Appl. Phys. Lett,* **69** (1996), p. 1220.
7. F. C. Frank and W. T. Read, in *"Symposium on Plastic Deformation of Crystalline Solids,"* Carnegie Institute of Technology, Pittsburgh, 1950, p. 44.
8. J. P. Hirth and J. Lothe, *"Theory of Dislocations"*, 2nd ed., J. Wiley, New York, 1981.
9. A. Einstein, *"Investigations on the Theory of Brownian Movement,"* Methuen, London (1926), p. 9.
10. J. Weertman and P. Shahinian, *Trans. A.I.M.E.* **209** (1957), p. 1298.
11. N. Louat and C. A. Johnson, *Phil. Mag.* **7** (1962), p. 2051.

OBSERVATION OF DISLOCATION DYNAMICS IN THE ELECTRON MICROSCOPE

B. W. Lagow*, I. M. Robertson*, M. Jouiad*, D. H. Lassila', T. C. Lee*, and H. K. Birnbaum*

* Frederick Seitz Materials Research Laboratory,
University of Illinois at Urbana-Champaign, Urbana IL 61801

' Materials Science and Technology Division,
Lawrence Livermore National Laboratory, Livermore CA 94550

ABSTRACT

Deformation experiments performed *in-situ* in the transmission electron microscope have led to an increased understanding of dislocation dynamics. To illustrate the capability of this technique two examples will be presented. In the first example, the processes of work hardening in Mo at room temperature will be presented. These studies have improved our understanding of dislocation mobility, dislocation generation, and dislocation-obstacle interactions. In the second example, the interaction of matrix dislocations with grain boundaries will be described. From such studies predictive criteria for slip transfer through grain boundaries have been developed.

INTRODUCTION

By performing dynamic experiments *in-situ* in a transmission electron microscope, it is possible to directly observe changes in microstructure caused by external stimuli. *In-situ* straining of materials is a particularly useful and illustrative example, as it provides the means to observe dislocation interactions and microstructure evolution dynamically. It is, however, important to be cognizant of the sample thickness, and of the influence the nearby surface can have on dislocation behavior.

Provided the observations are analyzed cautiously and comparisons are made with other techniques, *in-situ* deformation can provide useful insight to dislocation behavior. Such observations are particularly important to current efforts in multiscale modeling of deformation of materials, as they provide a means for testing the code output. The *in-situ* TEM deformation experiments also underscore the complex issues that must be addressed by a successful simulation.

In this paper, we present two examples of experimental results that would not have been possible without the *in-situ* TEM deformation technique. In the first, we discuss dislocation generation and work hardening in high-purity, single-crystal Mo, and in the second, slip transfer across grain boundaries.

EXPERIMENTAL PROCEDURE

The TEM straining samples typically have dimensions of 3 mm x 10 mm and are between 100 and 200 μm thick. The central portion of the rectangular specimen is thinned to electron transparency by conventional methods. *In-situ* straining was performed using a single-tilt straining stage and dynamic events were recorded through a TV-rate camera onto videotape. The single-tilt straining stage is designed so that one end of the sample remains fixed, while the other end is displaced.

RESULTS

Deformation in high-purity, single-crystal Mo

The Mo samples used in this investigation were zone-refined single crystals, UHV annealed at 850° C for 24h. Samples from one crystal contained a high dislocation density [1]. The dislocations were either isolated or arranged in tangles that were composed of intersecting a/2<111> perfect dislocations, with short a<100> junction dislocations forming at the intersections. These dislocation tangles were important as they acted as dislocation sources and as obstacles to mobile dislocations. In the initial stages of deformation, edge dislocation segments propagated from the tangles and trailed behind them long, straight screw dislocations, which are immobile at room temperature and at low stress [2]; see Figure 1 for an example. At higher stresses, the screw dislocations become mobile and initially moved smoothly on one slip plane. As the density of mobile dislocations increased and more interactions occurred, the dislocations cross-slipped to negotiate the obstacles. An example of cross-slip is shown in Figure 2 in which comparison images formed by superimposing a negative image (white dislocations) of a later frame on a positive image of an earlier frame are shown. The change in dislocation position as a function of time is apparent and corresponds to screw dislocations cross-slipping between {110} and {112} planes.

The series of video images presented in Figure 3 show two methods used by screw dislocations to overcome an obstacle; in these images the obstacles are not visible. Cusps are observed on the dislocations where they interact with a strong obstacle. The unpinned segments on dislocation 1 continue to slip past the obstacle and eventually the dipole is pinched off, allowing the screw dislocation to continue its motion. Dislocation 2 negotiates its obstacle differently, requiring cross-slip of a segment of the dislocation at the obstacle. As the line segment on the left of the cusp in 2 continues to slip, its edge component expands to produce the loop seen at $t = 7$ s. The segments pinch off and the screw dislocation again moves as a complete unit. It has also been observed [1] that if the length of the cross-slipped segment increases, the edge segments of the loop can act independently, moving away from the pinning point and trailing two screw dislocations behind them; i.e., a non-regenerative dislocation source operates. A similar source mechanism has been observed to operate in NiAl [3].

Dislocations also multiply by the action of pole sources (Figure 4) [1]. The screw dislocation is pinned at point T. A highly mobile edge segment is nucleated on the dislocation line, which moves away rapidly generating two screw dislocations, one of which remains pinned, while the other moves slowly away from the source. The source is thus reset, and the pinned screw dislocation nucleates an edge segment moving in the opposite direction. The conditions to generate this type of pole source are not yet known, although it is worth mentioning that the tangle shown in Figure 1 also became a pole source at higher strains.

In samples with a low initial density of isolated dislocations ($< 1 \times 10^8$ cm^{-2}), dislocation tangles form as mobile dislocations interact. As other dislocations impinge on the tangles they become pinned and bow out between the pinning points. The bowed segments contain edge dislocations that move rapidly away from the tangle, creating a mobile screw dislocation and leaving a dislocation in the tangle. Figure 5 shows an example of this increase in complexity with time. Although some dislocation tangles break up, in general the density and complexity of tangles increases with increasing strain.

These examples of dislocation generation, cross-slip, and dislocation interactions with obstacles and other dislocations illustrate the complexity of the problem facing the modeling community, if the simulations are eventually to be used to predict dislocation behavior and ultimately the stress-strain relationship of a material. The situation becomes more complicated if the deformation behavior in polycrystalline materials is to be simulated, as the interaction of dislocations with grain boundaries will need to be considered.

Dislocation interactions with grain boundaries

In general, grain boundaries act as barriers to dislocations, although under special circumstances (e.g., the line of intersection of the incoming and outgoing slip planes in the grain boundary plane are colinear and the line direction of the impinging screw dislocations is parallel to this line) the dislocations can pass unimpeded through the grain boundary. In most cases, the interaction with the grain boundary is more complex. Dislocations impinging on a grain boundary can enter the grain boundary where they can either retain their lattice Burgers vector [4], or dissociate to form perfect or partial grain boundary dislocations [5] or DSC dislocations [6]. The incorporated dislocations may be glissile or sessile in the grain boundary plane. The grain boundary can also eject dislocations into the neighboring grain (*slip transfer*) [7-11], although the site of the emitted dislocations need not be coincident with the entry point. Alternatively, a crack can nucleate and propagate along the grain boundary, leading to intergranular fracture [12-14]. The response of the grain boundary depends intimately on the orientation and chemistry of the grain boundary, and it can be altered by changing the boundary chemistry [15-17]. In Figure 6, we show one example [10] of slip transfer through a $\Sigma = 3$ grain boundary in 310 stainless steel in which two slip systems, A and B, impinged on the grain boundary. Dislocations were observed to emerge into the adjoining grain from different locations along the grain boundary; the primary emerging system is labeled D and the secondary system C.

To understand what controls the slip system activated by the grain boundary to allow slip transfer, three conditions were considered [10-11]: (a) the angle between the lines of intersection between the grain boundary and each slip system must be a minimum; (b) the magnitude of the Burgers vector of the dislocation left in the grain boundary must be a minimum; and (c) the resolved shear stress on the outgoing slip system must be a maximum. The result of applying these conditions to the situation shown in Figure 6 is given in Table 1. Slip system D is predicted if all three conditions are considered. The dislocations left in the grain boundary as a result of this emission process can slip in the grain boundary but their motion is impeded by the step in the grain boundary (marked by an arrow). Dislocations labeled C arise from the grain boundary emitting dislocations in response to the stress developed by the blocking of these grain boundary dislocations by the grain boundary step. These criteria have been applied to a number of grain boundary reactions in different materials and they have shown that, in general, a competition exists between criteria (b) and (c), and that it is these criteria that determine the outgoing slip system [11].

DISCUSSION

The experiments described above illustrate some observations made using the *in-situ* TEM deformation technique. The observations in Mo provide a clear picture of the processes of dislocation multiplication and work hardening in single-crystal Mo, and, by analogy, to many BCC materials in which cross-slip is possible and where there is a large differential between edge and screw mobility. These observations further indicate that understanding the physics of dislocation tangle structures is of primary importance in understanding the mechanical behavior of these materials. The slip transfer experiments made possible a model which not only accurately predicts the outgoing slip system, but which is independent of crystal structure, and is therefore likely applicable to many different materials.

CONCLUSIONS

The *in-situ* TEM deformation technique generates insights into the mechanical properties of materials, providing detailed information of dislocation dynamics, dislocation generation, and dislocation interactions with obstacles, other dislocations, and grain boundaries.

ACKNOWLEDGEMENTS

This work was funded by the Department of Energy under contract DEFG02-91-ER45349 and by Lawrence Livermore National Laboratory.

REFERENCES

1. M. Jouiad, B. W. Lagow, I. M. Robertson, and D. H. Lassila, in *Multiscale Phenomena in Materials: Experiments and Modeling,* D. H. Lassila, I. M. Robertson, R. Phillips, and B. Devincre, Eds. (MRS: Pittsburgh, 2000).

2. F. Louchet and L. P. Kubin, *Phys. Stat. Sol. A* **56** 169 (1979).
3. D. Caillard, in *High-Temperature Ordered Intermetallic Alloys VIII,* E. P. George, M. Yamaguchi, M. J. Mills, Eds. (MRS: Pittsburgh, 2000), p. 737.
4. W. Bollman, B. Michaut, and G. Sainfort, *Phys. Stat. Sol. A* **13** 637 (1972).
5. R. C. Pond, *Proc. Roy. Soc.* **A357** 471 (1977).
6. W. Bollman, *Crystal Defects and Crystalline Interfaces* (Springer-Verlag: New York, 1970).
7. J. D. Livingston and B. Chalmers, *Acta Metall.* **5** 322 (1957).
8. Z. Shen, R. H. Wagoner, and W. A. T. Clark, *Scripta Metall.* **20** 921 (1986).
9. Z. Shen, R. H. Wagoner, and W. A. T. Clark, *Acta Metall.* **36** 3231 (1988).
10. T. C. Lee, I. M. Robertson, and H. K. Birnbaum, *Phil. Mag. A* **62** 131 (1990).
11. W. A. T. Clark, R. H. Wagoner, Z. Y. Shen, T. C. Lee, I. M. Robertson, and H. K. Birnbaum, *Scripta Metall.* **26** 203 (1992).
12. G. M. Bond, I. M. Robertson, and H. K. Birnbaum, *J. Mat. Res.* **2** 436 (1987)
13. I. M. Robertson, G. M. Bond, T. C. Lee, D. S. Shih, and H. K. Birnbaum, *J. de Physique* **5** 677 (1988).
14. T. C. Lee, I. M. Robertson, and H. K. Birnbaum, *Acta Metall.* **37** 407 (1989).
15. R. H. Jones in *Mechanical Properties and Phase transitions in Engineering Materials: Earl R. Parker Symposium on Structure-Property Relationships*, S. D. Antolovich, R. O. Ritchie, and W. W. Gerberich, Eds. (TMS: Warrendale PA, 1986), p. 227.
16. D. H. Lassila and H. K. Birnbaum, *Acta Metall.* **35** 1815 (1987).
17. C. J. McMahon, Jr., *Materials Characterization* **26** 269 (1991).

Figure captions:

1. Propagation of edge dislocations in Mo away from a tangle at low stress. As the edge dislocations move, they trail long screw segments behind them.

2. Cross-slip of screw dislocations in Mo. The positive (black) image represents the initial position and the superimposed negative (white) image represents the final position in each picture. The angle of the shift in direction is consistent with cross-slip between (110) and (112) type planes.

3. Dislocation interactions with obstacles.

4. Operation of a dislocation pole source in Mo.

5. Build-up of a complicated tangle in Mo by dislocation multiplication. The final image shows the same tangle after additional straining.

6. Slip transfer at a $\Sigma = 3$ boundary in 310 SS. The pile-ups at A and B nucleate the dislocations at D and grain boundary dislocations; a pile-up in the grain boundary nucleates the dislocations at C [10].

Table 1: Parameters for prediction of slip transfer in the situation shown in Figure 6 [10].

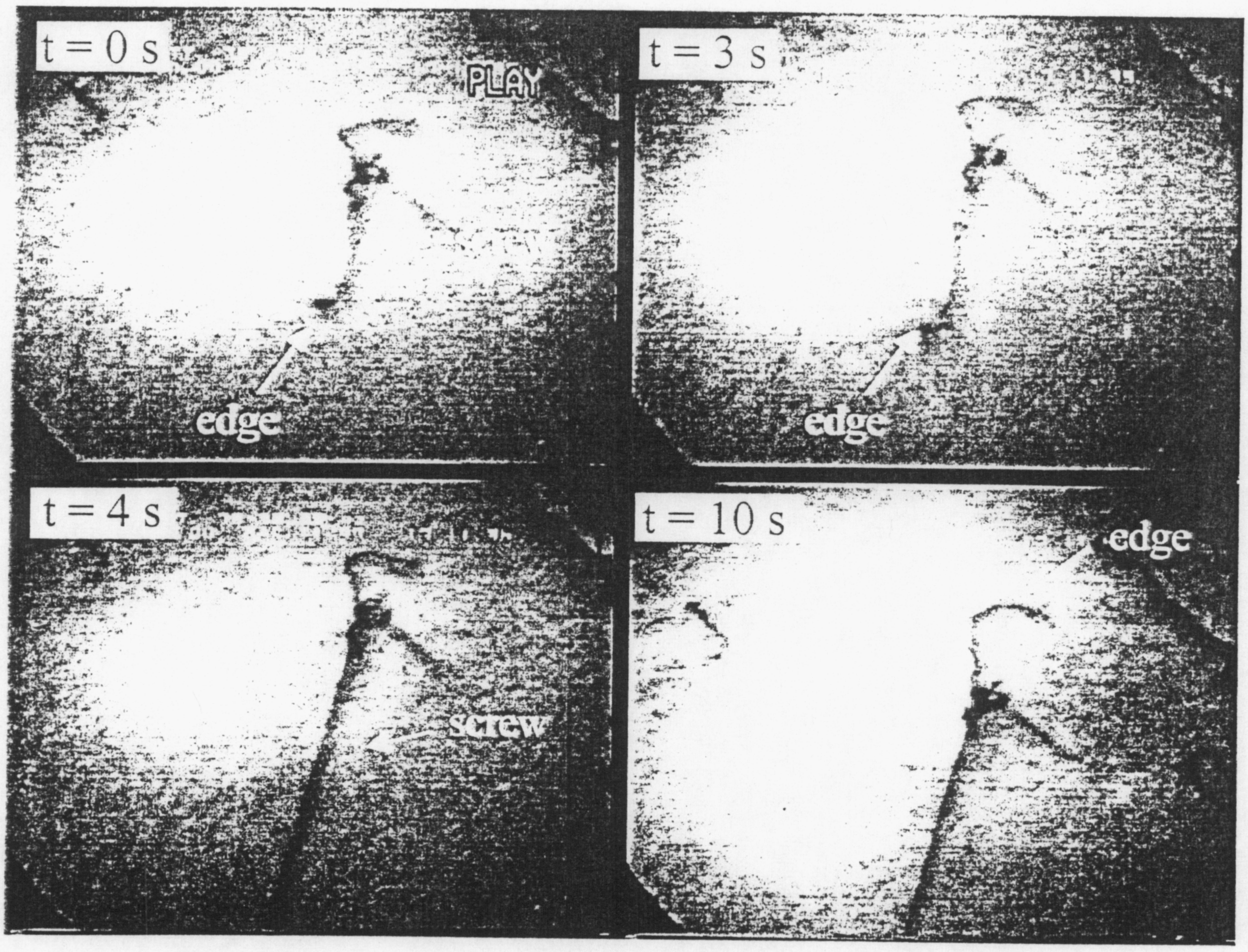
t = 0 s
PLAY
edge
t = 3 s
edge
t = 4 s
screw
t = 10 s
edge

Lagow et al Figure 1 of 6

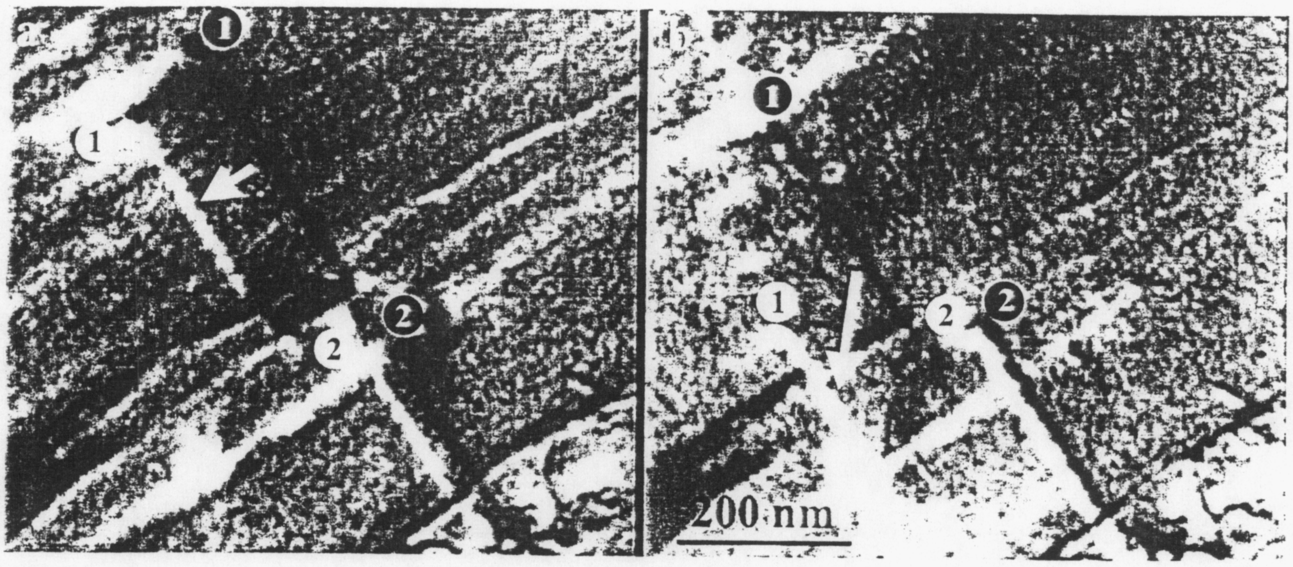
a
①
1
②
2
b
①
1
2
②
200 nm

Lagow et al Figure 2 of 6

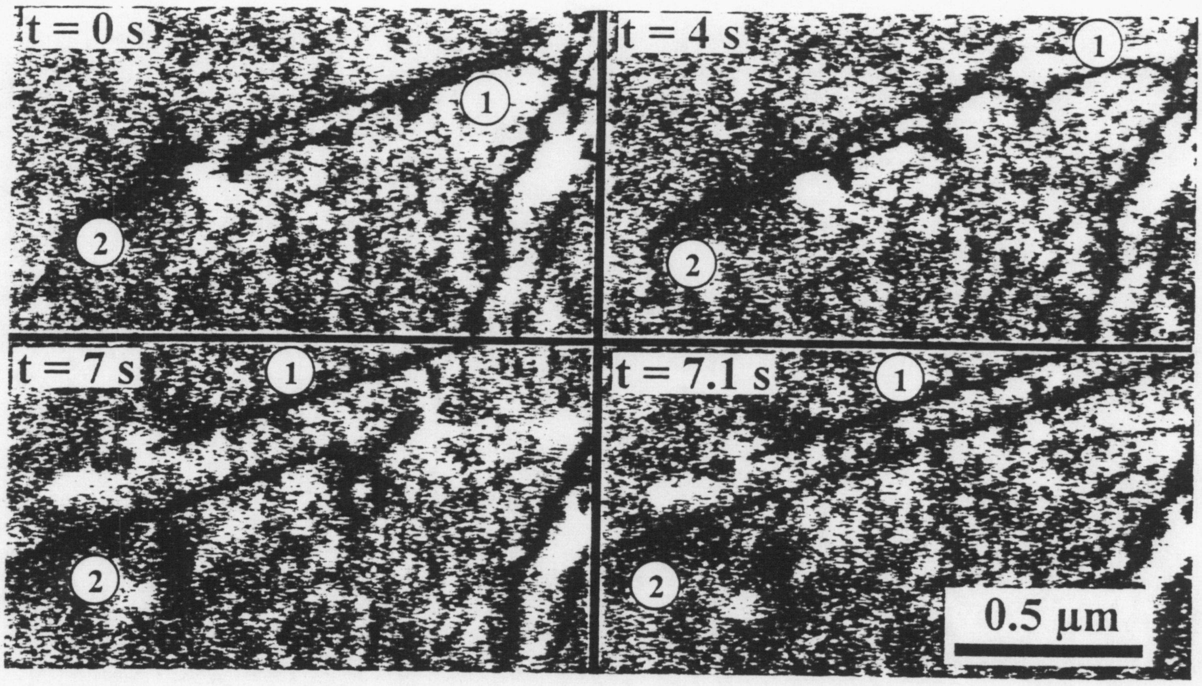
t = 0 s
t = 4 s
t = 7 s
t = 7.1 s
①
②
0.5 µm

Lagow et al Figure 3 of 6

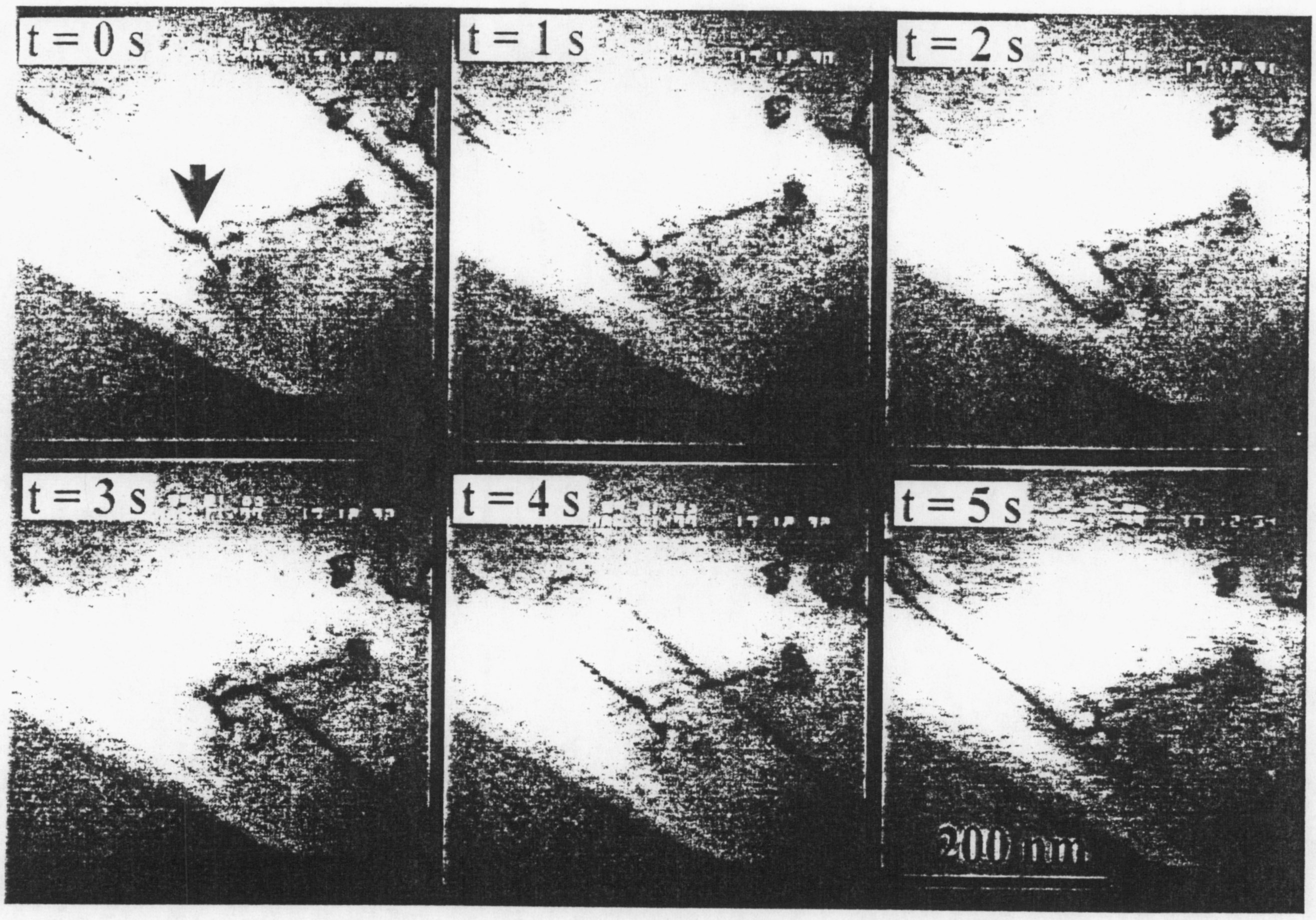

t = 0 s
t = 1 s
t = 2 s
t = 3 s
t = 4 s
t = 5 s
200 nm

Lagow et al Figure 4 of 6

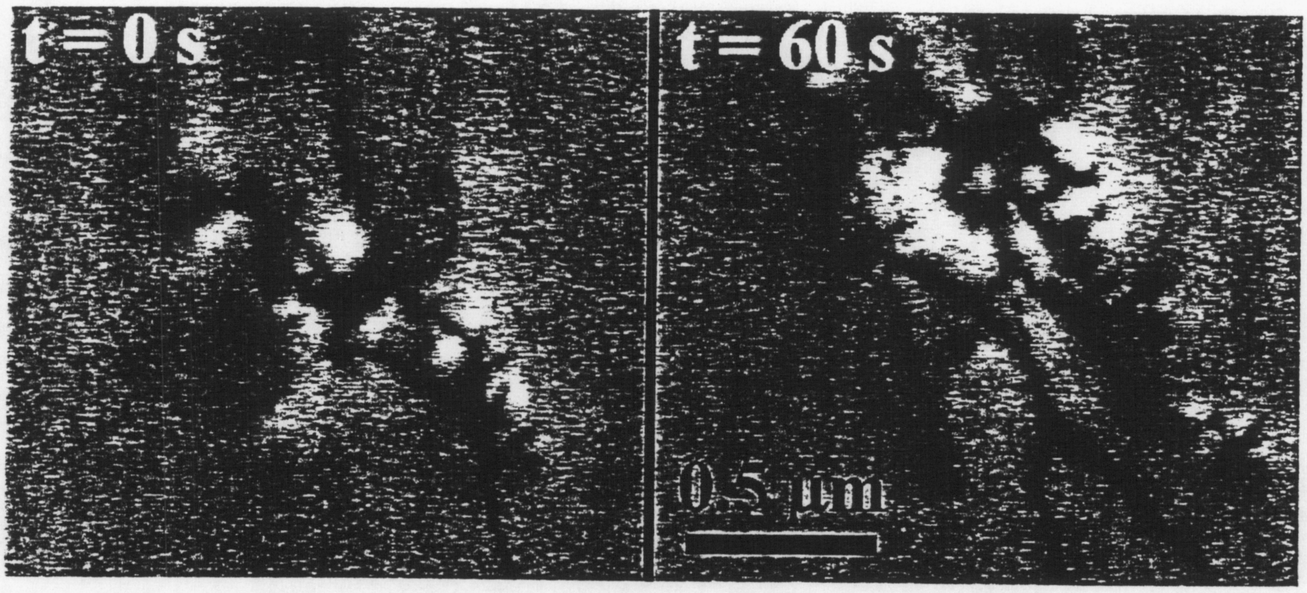
t = 0 s
t = 60 s
0.5 µm

Lagow et al Figure 5 of 6